Exploratory and Spatial Statistics for Evaluating Heat and Mass Transfer in Geothermal Areas

A Dissertation
Presented in Partial Fulfillment of the Requirements for the
Degree of Doctor of Philosophy
with a
Major in Geology
in the
College of Graduate Studies
University of Idaho
by
Cary Lindsey

Major Professor: Jerry Fairley, Ph.D.
Committee Members: Peter Larson, Ph.D.; Leslie Baker, Ph.D.; and
Christopher Williams, Ph.D.
Department Administrator: Leslie Baker, Ph.D.

May 2018

Authorization to Submit Dissertation

This dissertation of Cary Lindsey, submitted for the degree of Doctor of Philosophy with a Major in Geology and titled "Exploratory and Spatial Statistics for Evaluating Heat and Mass Transfer in Geothermal Areas," has been reviewed in final form. Permission, as indicated by the signatures and dates below, is now granted to submit final copies to the College of Graduate Studies for approval.

Major Professor: _____Date_____
        Jerry Fairley, Ph.D.

Committee
Members: _____Date_____
        Peter Larson, Ph.D.

        _____Date_____
        Leslie Baker, Ph.D.

        _____Date_____
        Christopher Williams, Ph.D.

Department
Administrator: _____Date_____
        Leslie Baker, Ph.D.

Abstract

The movement of heat and fluid in geothermal systems is complex. Over the past 75 years, many scientists have applied a variety of tools to constraining the heat and mass transfer in these systems. Refined measurements of this transfer allow for better characterization of geothermal systems, sustainable production of geothermal energy resources, and enhanced modeling of reservoirs.

In this dissertation, I offer a progression of tools for measuring and/or calculating surface heat flux in the Yellowstone Caldera. Testing of a novel calorimeter, the Ice Box Calorimeter, to measure surface heat flux is discussed in Chapter 1. This calorimeter was an early project in my graduate career and while it was ultimately unsuccessful for measuring heat flux in my field site, it was beneficial for learning the nuances of heat transfer. Chapter 2, provides a dimensional analysis approach for calculating the conductive heat flux at the ground surface by treating the surface as a Robin, or convective/conductive, boundary. By using this convention, I am able to solve for the convective heat flux and relate it to the conductive heat flux in the field. Finally, in Chapter 3, a multivariate statistical approach is taken using aqueous samples collected in Pocket Basin in the Lower Geyser Basin of Yellowstone National Park, to make inferences regarding spring connectivity and fluid flow pathways in the area. The statistical approach is compared to standard geochemical tools and temperature contour maps created from shallow subsurface temperatures collected in the field.

Acknowledgements

The journey to this dissertation has been greatly fortified by the guidance and inspiration of Dr. Jerry P. Fairley. His sense of adventure in science is contagious and I hope to pass that along to others. Thank you.

Many thanks also go to my committee who represent excellence in their own fields and expect it from me in mine. I would also like to thank my undergraduate mentors and advisors for encouraging me along this journey. Each has played a pivotal role in my success.

Special recognition must go to my fellow graduate students who have been a valuable source of support and collaboration, specifically among them I must mention Brady Lubenow, Adam Price, and Meg Aunan. Thank you all so much. I look forward to collaborating with you for many years to come.

Dedication

Dedicated in loving memory to Ruth Lindsey, my number one fan; and to my clan – my three amazing children who keep me on track and going for the epidote; my father whose pride in me keeps me striving to be everything he thinks I can be, my sister who spent many days babysitting and caring for us whether we were down the street or across the country, and my mother who has loved and supported me at my best and worst. Thank you for always believing in me. This is for you. - CL

Table of Contents

List of Figures

List of Tables

<div align="center">

Chapter 1

ICE BOX CALORIMETRY: A TEST OF APPLICABILITY IN NON-STEAMING GEOTHERMAL AREAS

</div>

1.1 Abstract

Surface heat flux, an important tool for characterizing geothermal areas, is often difficult, if not impossible, to measure directly. In this study we present an analysis of icebox calorimetry (IBC), a method that has, to date, been used only in geothermal areas with steaming ground. We test the method in varied geothermal environments and present possible refinements, pitfalls, and suitable applications. The ability to calculate even a rough estimate of surface heat flux can allow enhanced exploration of geothermal energy systems and aid in the constraint of heat flux in geothermal areas.

1.2 Introduction

Heat flux is defined as the heat transfer rate per unit area perpendicular to the direction of transfer (Incropera and Dewitt, 2007). In geothermal systems, heat flux is a valuable tool for exploration, but is difficult to measure directly. One flux mechanism that can be especially difficult to measure is surface heat flux or conductive heat flux from the ground. In areas where wells have been drilled for oil and gas or geothermal exploration, it is often possible to calculate conductive heat flux based on the geothermal gradient calculated when the well hole is logged. Many areas, however, do not have a sufficient number of wells to calculate a representative geothermal gradient. Drilling for the purpose of exploration is costly and is a tool not available to many researchers. For this reason, researchers often seek less expensive and easy to deploy tools for measuring heat flux. Calorimeters are one such tool.

Calorimeters can be used to measure surface heat flux and attempts have been made to use them in geothermal areas to measure heat flux for over 50 years, specifically in areas with high flux values. R.F. Benseman (1959) developed an open air calorimeter to measure the output of heat from the ground in thermal areas. The benefits to Benseman's calorimeter are that it didn't require the ground surface to be disturbed as in the case with previous calorimeters, the flow of steam should not be affected, and it was light and portable. The calorimeter was tested in areas with very little to no surface vegetation. Benseman reported heat flux values of approximately 21 W/m^2 at the low end to almost 3,000 W/m^2 at the high end. Reported accuracy was about 10% for values above about 420 W/m^2 and values below that were quite noisy with an accuracy of $\pm$ 42 W/m^2. While there was measured success with the Benseman device in the higher heat flux ranges, he noted several potential problems among them windy conditions and variations in ambient temperatures throughout the day.

Dawson (1964) discusses both the calorimeter of Benseman and his own venturi meter for measuring heat flux through the soil (Benseman's for lower values, the venturi meter for higher), but noted that both are slow and require skilled operation. For this reason, he suggested them as a means simply to calibrate indirect measurements that can be taken rapidly with less complex equipment.

D.E. White (1969) suggested snowfall as a calorimeter and used this method in Yellowstone National Park. However, this method requires "optimum" conditions such as 0 °C temperatures before, during, and after snowfall; snowfall of greater than 10 cm in a less than 24 hour period; and an area relatively bare of vegetation. Despite errors and uncertainty as well as the precise conditions needed for use, White suggests the calorimeter does provide a means of recognizing local changes in heat flux.

A more recent calorimeter was designed by Hochstein & Bromley (2005) and used to measure heat flux of steaming ground in Karapiti, New Zealand. The goal for this new calorimeter was to reduce the scatter noticed in the Benseman (1959) field tests while still maintaining a compact, easy to deploy unit. The calorimeter was not open air like the Benseman device but instead used water as the transfer medium. The results of the study in Karapiti showed good

reproducibility of conductive heat flux but inconsistent results with the advective heat flux.

Terada et al. (2008) suggest a new calorimeter that seeks to avoid many of the pitfalls of the previous calorimeters. The Ice Box Calorimeter (IBC) has been used with reported success in steaming ground of an active volcanic area in Japan (Terada et al., 2008). The calorimeter consists of two identical pans with an equal mass of ice in each. One pan is placed directly on the ground with grass or other obstructions removed to ensure maximum contact with the surface. The other pan is placed on an insulating material so that it does not contact the ground surface. Apart from the heat flux from the ground surface, each pan experiences the same heat transfer mechanisms – evaporation, radiation, conduction, and convection. Assuming all else to be equal, the difference in the melt water of the two pans represents only the heat flux from the ground surface. Using the difference in the mass of the melt water, heat flux can be calculated as follows:

$$q = \frac{Lm}{At}, \tag{1.1}$$

where q is the heat flux (W/m^2), L is the latent heat of fusion of water ($3.34x10^5 \frac{J}{kg}$), m is the mass of the melt water in the insulated pan subtracted from the non-insulated pan (kg), A is the area (m^2), and t is time (s).

As our field site in Yellowstone is an active geothermal area with indication of high heat flux, up to 20 W/m^2 according to ASTER and MODIS thermal infrared data presented by Vaughan et al. (2012), we decided to try the IBC as a tool for calculating heat flow from the ground surface. The encouraging results for measuring conductive heat flow with the Hochstein & Bromley (2005) calorimeter suggest measuring the conductive heat flux may be possible with a calorimeter placed directly on the ground surface even if the surface has been disturbed. Here, we present our process of refining our collection techniques with the IBC and subsequent results.

FIGURE 1.1: Ice Box Calorimeter setup near Borax Lake, Alvord Basin, OR

1.3 Field Applications

1.3.1 Borax Lake

We tested our setup of the ice box calorimeter in the Borax Lake area of the Alvord Basin in southeast Oregon in the spring of 2014. The area is host to approximately 175 geothermal springs along a northeast/southwest left stepping fault extending over 1 kilometer. The Alvord Basin is a north-south trending graben associated with the Basin and Range Province and is flanked by the Steens and Pueblo mountains to the west and the Trout Creek Mountains to the east (Jerry P. Fairley and J. J. Hinds, 2004).

For each calorimeter, we used two 9-inch anodized aluminum pans with 800 grams of water frozen in each (Figure 1.1). The heat flux was calculated at five random locations within a 100-meter by 100-meter grid.

As can be seen in Table 1.1, the results of the calculations were inconclusive. For four of the five locations, a negative heat flux was calculated (i.e. more melt water in the insulated pan). In one location, a positive heat flux of 108 W/m^2 was calculated. The location of this calorimeter had been shown in a ground temperature survey to have higher temperatures than the surrounding locations. We determined from the field trial that the IBC, as it was, was not

TABLE 1.1: IBC results for field trial at Borax Lake.

Location	Coordinates	Δ Water (g)	Heat Flux (W/m^2)
1	(24, 9)	-0.004	-14.203
2	(57, 69)	0.0306	108.653
3	(39, 75)	-0.0224	-79.537
4	(36, 36)	-0.0062	-22.015
5	(24, 93)	-0.0022	-7.812

suitable for this application – either the area did not have sufficient heat flux for the IBC to function properly and some threshold value must be exceeded or each pan was not experiencing identical heat transfer apart from the ground surface flux. A decision was made to attempt to refine the technique in the lab before another field trial.

1.3.2 Lab Trials

In the lab, we set up a mock thermal area (Figure 1.2) using a heat source (hot plate) and an aluminum pan filled with sand. The sand was neither wetted nor dried. Terada et al. (2008) set up a similar experiment with wet sand. The temperature was logged at the bottom, midpoint, and surface of the sand. These temperatures were used to calculate the maximum expected heat flux. We ran this scaled down version of the IBC four times. Each time the calculated heat flux exceeded our maximum expected heat flux. Our thought was that storage of heat in the subsurface might be a factor and what we were seeing was mined heat; however, we felt that we could model the storage and remove that from the calculation so we proceeded with refining the setup. We chose three variations of the IBC to test in the field in the hopes of counteracting atmospheric disturbances. We tested one setup with a large cooler around the IBC, one that had a vented box over the IBC, and the original as used in the Alvord Basin. We proceeded to a second field trial with these three setups.

1.3.3 Vulcan Hot Springs

We tested all three variations of the IBC at Vulcan Hot Springs in the Payette National Forest of Idaho. Logging the temperature inside of the box was necessary to ensure that we were
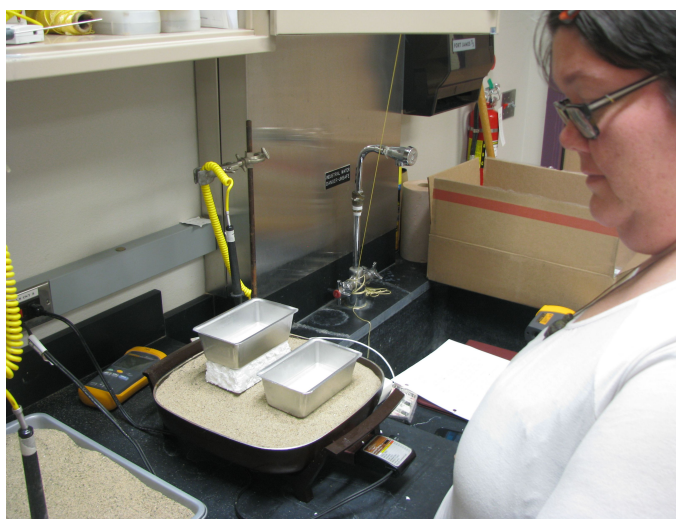
FIGURE 1.2: Lab ice box calorimeter setup

not inducing heat flow. We determined that the cooler enclosed set up could induce heat flow as the internal temperature of the cooler quickly dropped below ambient temperatures and thus changed temperature gradient. The vented box enclosed IBC (Figure 1.3) did not experience such temperature drop. All calculated heat fluxes were positive; however, we felt that the vented box, with near atmospheric temperatures inside of the box, gave the most trusted measurement. The heat flux from the vented box was approximately 150 W/m^2.

1.3.4 Yellowstone

In July of 2014, as part of a larger project funded by the National Science foundation, our team implemented the refined IBC in the Morning Mists springs area of the Lower Geyser Basin in Yellowstone National Park. We chose 18 locations at random locations on the predetermined temperature collection grid, six per location. The calculated heat fluxes ranged from -2.12 W/m^2 to 344 W/m^2. The negative measurement was taken as a rainstorm moved in and the wind was making it difficult to stabilize the IBC setup. The mean heat flux was 155 W/m^2. This is excessive heat flux even for the Yellowstone Caldera. Vaughan et al. (2012) shows an average radiative heat flux of the same area ranging from 0 to 30 W/m^2.

FIGURE 1.3: Ice Box Calorimeter at Vulcan Hot Springs

We plotted the heat flux values and compared these to plots of temperature and thermal conductivity of the same area (Figure 1.4). The heat flux plot seems to show no correlation with the temperature plot or the thermal conductivity plot further suggesting unreliable results.
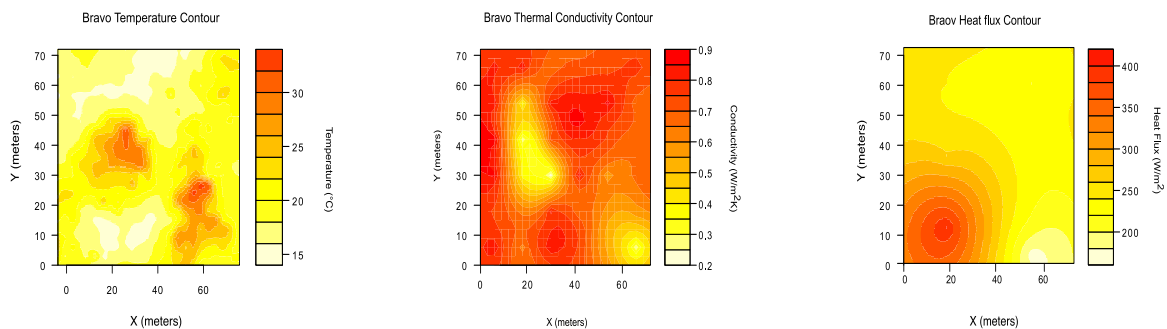
FIGURE 1.4: Contour maps for Bravo: a) shallow ground surface temperatures, b) thermal conductivity, and c) heat flux.

1.4 Discussion and Conclusions

For all three field experiments we calculated positive heat flux values based upon the melt water difference. The heat flux values were all within similar ranges despite coming from three

very different thermal regimes and all were excessive. Focusing on the heat flux calculations at Yellowstone National Park, those considered to be from the refined IBC, we calculated a mean heat flux of 155 W/m^2. This is above the average heat flux of the caldera and the Morning Mist Springs area is not one of the hotter areas of the park as compared to the vapor dominated systems of the Mud Volcano area and Norris Geyser Basin. This, coupled with the fact that Vulcan Hot Springs and the lab experiment gave similar values, suggests that this calorimeter is not appropriate for measuring the heat flux in the test areas. It is possible that all three areas are dominated by conductive heat flux which Terada et al. (2008) suggests could be problematic; however, Hochstein & Bromley (2005) seemed to have better results in conductive areas.

It may be the case that the necessary caveats mentioned for the Hochstein & Bromley calorimeter (2005) and the White calorimeter (1969) should be applied to the IBC. Hochstein noted that after disturbance of the ground, it was ideal to allow the area to be undisturbed for up to a full day to return to equilibrium. Virtually no time was allowed during our application of the IBC and Terada et al. (2008) make no mention of allowing equilibration time in their study. White mentioned the need for 0 ° C temperatures before, during, and after application of the snowfall calorimetry to avoid mining of heat stored in the shallow subsurface. The snowfall calorimeter seems most similar to the IBC in theory and I would suggest that this parameter may have had the most impact. For steaming areas, Dawson (1964) also suggests that calorimeters prevent access to the advective impacts of the air thus causing water vapor to condense in the soil because the temperature has dropped below boiling. This condensation continues until enough heat is provided to raise the temperature back to boiling. This may have also affected the IBC in it's original deployment.

In conclusion, the IBC was not successful in measuring heat flux in the three field sites presented in this study. Limitations of other calorimeters discussed in the study and the results of our field research also suggest that the initial IBC results may be flawed as they do not take into account the impacts of meteorological conditions at the surface or calorimeter's impact on the heat transfer at the surface.

Chapter 2

CALCULATING SURFACE HEAT FLUX IN GEOTHERMAL FIELDS USING THE NUSSELT NUMBER: CASE STUDY MORNING MIST SPRINGS, YELLLOWSTONE NATIONAL PARK

2.1   Abstract

Conductive heat flux in thermal areas of Yellowstone National Park is a difficult parameter to measure. Having the thermal gradient is considered necessary and this is often only acquired by drilling and temperature logging a drill hole. As an alternative, I used dimensional analysis to solve for the Nusselt number, the dimensionless parameter representing the ratio of convection to conduction in a fluid, and applied Robin boundary conditions to calculate conductive flux at the ground surface in the Morning Mist Springs area of Lower Geyser Basin, Yellowstone National Park. Constraining this flux has implications for calculating the total heat budget of the Yellowstone caldera and for applications in exploration and sustainable exploitation of geothermal energy systems.

2.2   Introduction

Quantification of heat flow in geothermal fields is important for resource characterization and management (Dawson, 1964; Yuhara, 1970; Seward et al., 2018), and increased accuracy of resource parameters such as heat flow can lead to "improved calibration of geothermal reservoir models" (Bromley et al., 2011). In areas such as Yellowstone National Park, where production management isn't the driver, monitoring of the heat flow is important for recognizing fluctuations or changes in the geothermal system (Vaughan et al., 2012) and for understanding the structural evolution of the caldera (Morgan et al., 1977). Because heat flow is such an important parameter, much work has been done to quantify it; however, problems still exist. The heat transfer mechanisms at play in geothermal fields are many and not all are easily measured.

According to Dawson (1964), heat discharge from geothermal systems is comprised of the following mechanisms:

1. heat flow through the soil,

2. heat loss from water surfaces,

3. fumaroles,

4. discharge from geysers and springs, and

5. seepage to nearby water bodies such as streams and lakes.

Sorey and Colvard (1994) proffer the following formula to capture the total heat flow:

$$H_{tot} = H_{fum} + H_{adv} + H_{evap} + H_{rad} + H_{cond} + H_{gr}, \tag{2.1}$$

where H_{fum} is the differential advective heat loss in fumaroles, H_{adv} is advective heat loss in streams and springs, H_{evap} is the evaporative heat loss from water surfaces, H_{rad} is the radiative heat loss from water surfaces, H_{cond} is conductive heat loss from water surfaces, and H_{gr} is the heat flow from bare ground by convection, evaporation, and conduction.

Not all of conditions of heat transfer exist in all geothermal fields. For example, the field site described by Lubenow et al. (2016) has no steaming ground or fumaroles and thus no H_{adv} component. (For the interested reader, both Dawson 1964 and Sorey & Colvard 1994 discuss techniques for measuring heat flow from fumaroles).

One difference to notice between Dawson and Sorey & Colvard is seepage to nearby water bodies. Sorey & Colvard include this in H_{adv} whereas Dawson lists this component separately. Previous researchers have attempted to calculate the heat flux from geothermal using the chloride mass balance method from the major streams leaving the the system (Ellis and Wilson, 1955; R. Fournier, D.D. White, and A. Truesdell, 1976), in which case the seepage would be included in that calculation.

To calculate heat loss from the water surface, Dawson (1964) and Sorey & Colvard (1994) provide semi-empirical formulas for evaporative, radiative, and conductive heat loss at the surface. Those formulas are not included here but but it is enough to say that field measurements of water temperature and meteorological conditions are required, and these measurements are readily collected with the appropriate field equipment. McMillan et al. (2018) uses a deuterium doping method to calculate heat and mass flow of the springs combining H_{evap}, H_{rad}, and H_{cond} into one value.

The only component of the Sorey & Colvard equation left is H_{gr} or heat from the ground. As mentioned previously, this component has multiple heat transfer mechanisms. There can be an advective component, such as in areas of steaming ground, and a conductive component that is controlled by the heat source and soil/rock properties. Heat flow at the ground surface is also complicated by the issue of storage which is a factor of the Biot number (Price, Lindsey, and Jerry P. Fairley, 2017) (ratio of convection to conduction at the air/surface boundary) and the impacts of seasonal/diurnal influences.

Here, I present a novel method of calculating the conductive heat flux at the ground surface using shallow ground temperature and meteorological measurements by treating the surface as a conductive/advective (Robin) boundary. By treating the boundary as a Robin boundary, where the advective and conductive fluxes must be equal, it is possible to solve for the advective component by calculating the Nusselt number (ratio of advective/conductive heat flow of the air) thus quantifying the conductive component as well.

2.3 Site Description

The study area is located in the Morning Mist Springs area of Lower Geyser Basin in Yellowstone National Park. Lower Geyser Basin is the largest hydrothermal area in Yellowstone National Park and discharges more hot water than any other area of the Yellowstone caldera (Marler, 1964). The basin is home to hundreds of thermal features, including geysers, hot springs, and mud pots, the most common being neutral chloride-rich springs. Surficial sediments in the

FIGURE 2.1: Photo of field area taken from Porcupine Hill facing east.

Lower Geyser Basin consist of glacial and alluvial sediments, as well as deposits of precipitates from thermal discharge (L.J. Muffler et al., 1982). Rhyolite plateaus ranging from 120 to 300 meters high surround the basin with ages of the flows ranging from 120,000 to 600,000 years (L.J.P. Muffler, D.E. White, and A. Truesdell, 1971).

The Morning Mist area is located about 0.5 kilometers off Grand Loop Road just off the west end of the Mary Mountain Trail head, south of Nez Perce Creek and east of Porcupine Hill. The area is a flat, grassy plain dotted with thermal features (Lubenow et al., 2016). The area of my study contained one major spring, Bravo, and five or six smaller, subsidiary springs. Near the springs, deposits of sinter can found and lightly colored silt is deposited in the flat marshy areas. The area is surrounded by sands and gravels from the Pinedale Glaciation (L.J. Muffler et al., 1982). An image of the area taken from Porcupine Hill can be seen in Figure 2.1 and a map of the field site is given in Figure 2.2.
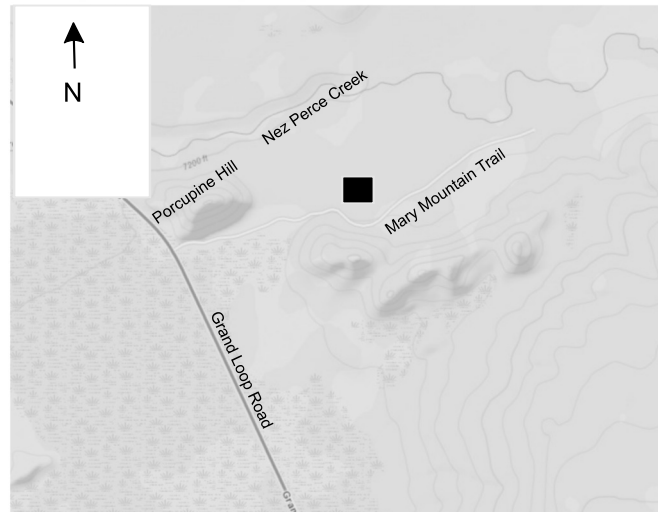
FIGURE 2.2: Approximate field location of Bravo field site.

2.4 Methods

2.4.1 Ground Temperature Measurements

Shallow subsurface temperatures were collected on a 72 x 72 meter grid. I used 20 centimeter Omega Rugged Penetration Thermocouple Probes (K-type) with a "T" handle connected to Fluke 51 II single input digital thermometers with a reported accuracy of $\pm 0.05\% + 0.3\,^{\circ}\mathrm{C}$ to record temperatures at 3 meter intervals. A geostatistical analysis was performed on the collected temperatures to look for spatial correlation. This involved computing the square of the difference in temperature between pairs of collected ground temperatures and plotting them as a function of their separation distance. The resulting variogram was fit with a variogram model. Fitting a model is necessary so that the parameters of variogram, the nugget, sill, and range, can be input into the kriging function, thus including the spatial correlation structure in the interpolation. The most common variogram models are spherical, Gaussian, exponential,

and power models. For further information regarding development of this method and selection of model fit, see Fairley et al. (2003) and others (e.g., Heffner and J. Fairley, 2006; Anderson and Jerry P. Fairley, 2008; Lubenow et al., 2016)

2.4.2 Air Temperatures

Air temperatures were recorded at 45-second intervals over a 7-day period. I used a Fluke beaded thermocouple with a range of -40 to $260\,°\mathrm{C}$ and a reported accuracy of $\pm 1.1\,°\mathrm{C}$.

2.4.3 Nusselt Calculation

A Robin boundary, or advection/conduction boundary, is defined by the following equation (Jerry P. Fairley, 2016):

$$-k_T \frac{dT}{dz}(z = 0, y, t) = h[T(z = 0, y, t) - T_\infty], \tag{2.2}$$

where k_T is the thermal conductivity of the solid, $\frac{dT}{dz}$ is the thermal gradient of the solid, h is the coefficient of convective heat transfer, T is the surface temperature of the solid, and T_∞ is the air temperature. The left–hand side represents conductive heat transfer at the boundary and the right–hand side represents advective heat transfer at the boundary. As can be seen from the equation, advective flux and conductive flux are equal under Robin boundary conditions. Solving for the right-hand side of the equation involves parameters currently unavailable for the field site – specifically, the geothermal gradient. For this reason, it is necessary to solve the right-hand side of the equation. Air temperatures and ground temperatures were collected in the field; therefore; therefore, the only missing parameter is h or the coefficient of convective heat flux. Using dimensional analysis, h can be calculated by first solving for the average Nusselt number. The Nusselt number is a dimensionless heat transfer parameter that represents the ratio of convective to conductive heat flux in a fluid, in this case, the air. The Nusselt number

is related to h by the following equation:

$$Nu_L = \frac{hL}{k},\qquad(2.3)$$

where h is the advective heat transfer coefficient, L is the characteristic length, and k is the thermal conductivity of the air. Rearranging this formula, I can solve for h:

$$h = \frac{Nu_L k}{L}.\qquad(2.4)$$

The Nusselt number can also be a function of the Rayleigh and/or Prandtl numbers, two other dimensionless parameters in heat transfer. The Rayleigh number is typically thought of as defining the flow regime, laminar or turbulent, of a fluid and the Prandtl number is the ratio of viscous and thermal diffusivity of a fluid. Nusselt number correlations are empirically derived based upon geometry and flow regime. Common geometries are vertical plates, cylinders, and horizontal plates. For this study, we use a horizontal plate geometry with a horizontal plate of length L, with L being the distance of spatial correlation as defined by the range of the semivariogram. For a horizontal plate with a Rayleigh number between 10^7 and 10^{11} (which will be shown true in the following calculations), the Nusselt number is only a function of the Rayleigh number and the empirically derived correlation equation for the average Nusselt number is (Incropera et al., 2007):

$$Nu_L = 0.15 Ra_L^{1/3},\qquad(2.5)$$

It should be noted that I am solving for Nu_L, or the *average* Nusselt number. The average Nusselt considers the field as one body whereas Nu_x, the local Nusselt, uses the distance from the surface boundary to the point of interest for the calculation (x) as stated below:

$$Nu_x = \frac{hx}{k},\qquad(2.6)$$

where h is the coefficient of convective heat transfer, x is the distance from the surface boundary to some point of interest, and k is the thermal conductivity of the fluid.

The following variables are needed to calculate Nu_L using the method outlined in this paper:

- x coordinate on grid;

- y coordinate on grid;

- temperature (°C) at 20 cm depth, $T_{(z=20)}$ for all x and y pairs;

- air temperature, T_{inf} (°C), for times of $T_{(z=20)}$ measurement;

- film temperature (the average of the surface and air temperatures), T_f (°C), for all x and y pairs, calculated using the following formula:

$$T_f = \frac{T_{(z=20)} + T_{inf}}{2};$$ (2.7)

- thermal conductivity of fluid (k_{fluid} in W/mK), based upon average air temperature from Incropera et al. (2007);

- fluid density (ρ_{fluid} in kg/m^3), calculated using the formula for dry air density; [1]

$$\rho = \frac{p}{R_{sp}T}$$ (2.8)

where p is air pressure in Pascals, R_{sp} is the specific gas constant for dry air, 287.058 J/kgK, and T is temperature in Kelvins;

- dynamic viscosity of fluid in kg/ms (μ) obtained from linear regression of tabulated data for dynamic viscosity (Incropera et al., 2007):

$$\mu = -8.3123 \times 10^{-12} \times T + 4.4156 \times 10^{-8} \times T + 6.2299 \times 10^{-6},$$ (2.9)

---

[1]It would be preferable to use the equation for moist humid air; however, for the temperature range during field collection, the air density when calculated from 0% humidity to 99% humidity changed less than $0.01 kg/m^3$ so I believe this to be an acceptable solution.

where T is temperature in Kelvins;

- specific heat of fluid in J/kgK (C_p), obtained from linear regression of tabulated data from specific heat (Incropera et al., 2007):

$$C_p = 7.875 \times 10^{-6} \times T^2 + 0.1712 \times T + 949.72;$$ (2.10)

- kinematic viscosity of fluid in m^2/s (ν), calculated from the following equation:

$$\nu = \frac{\mu}{\rho};$$ (2.11)

- thermal diffusivity of fluid in m^2/s (α_{fluid}), calculated using the following equation:

$$\alpha = \frac{k}{\rho C_p};$$ (2.12)

- thermal expansion of fluid in 1/K (β), calculated using the following equation:

$$\beta = \frac{1}{T_{(z=20)}},$$ (2.13)

where $T_{(z=20)}$ is in Kelvins;

- the Prandtl number (Pr), calculated using the following equation:

$$Pr = \frac{C_p \mu}{k};$$ (2.14)

- characteristic length in meters (L), given by the formula:

$$L = \frac{A_s}{P}$$ (2.15)

, where A_s is the area of the horizontal plate and P is the perimeter.[2]

---

[2]The theoretical horizontal plate in this case is constructed using the range of spatial correlation of temperatures squared as A_s and the perimeter is that range times four.

- Grashof number (*Gr*), the ratio of the force of buoyancy and viscosity on a fluid, calculated using the following formula:

$$Gr = \frac{g\beta(T_{(x=L)} - T_\infty)L^3}{\nu^2};$$ (2.16)

and finally,

- the Rayleigh number (*Ra*) given as:

$$Ra = GrPr.$$ (2.17)

The equations given above, in this order, end with the calculation of the Rayleigh number which is then used in Equation 2.4.3 to solve for the average Nusselt number. This number in turn, is used to solve for the coefficient of convective heat flux in Equation 2.4. Finally, plugging the values for *h* into Equation , we solve the right-hand side of the equation and in doing so solve the left-hand side as well giving a conductive heat flux value at each point.

2.5 Results

2.5.1 Ground Temperature Measurements

Over 600 shallow-subsurface temperatures were recorded over the 72 meter x 72 meter field area. As outlined in the methods, the spatial correlation structure of the temperatures was determined using geostatistical analysis. The plotted variogram can be seen in Figure 2.3. The best model fit is a spherical model with a nugget of 0.25, a sill of 14, and a range of 27 meters. The formula for the spherical model can be seen in Equation 2.18. Once the spatial correlation structure was included in the kriging function, a contour map of temperatures was generated (Figure 2.4). The analysis was done using R (R Core Team, 2014) and the script for the process
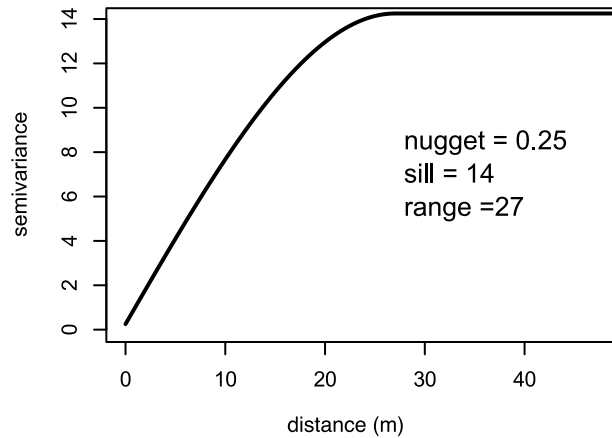
FIGURE 2.3: Omnidirectional variogram of ground temperature measurements.

can be seen in Appendix A.1.

$$\gamma(h) = \begin{cases} c\left[1.5\left(\frac{h}{a}\right) - 0.5\left(\frac{h}{a}\right)\right], & h \leq \alpha \\ c, & h > \alpha. \end{cases} \tag{2.18}$$

2.5.2 Nusselt Calculation

Once the Nusselt number calculation was applied to the temperature data, it was discovered that some Nusselt values were negative (i.e. the air temperature was hotter than the ground temperature) and could not be used to calculate the conductive heat flux. In the areas where the flux is negative, it represents flux into the ground. For this study, the focus is on the flux *from* the geothermal system, so I eliminated those values. Further examination may show that there is some dampening of the flux due to this and I hope to address that in subsequent investigations. All calculated positive values for the Nusselt calculation can be seen in Appendix B. As with the temperature measurements, it was necessary to determine any spatial correlation in the data. The same methods applied to the temperature data were applied to the flux values. Again, the
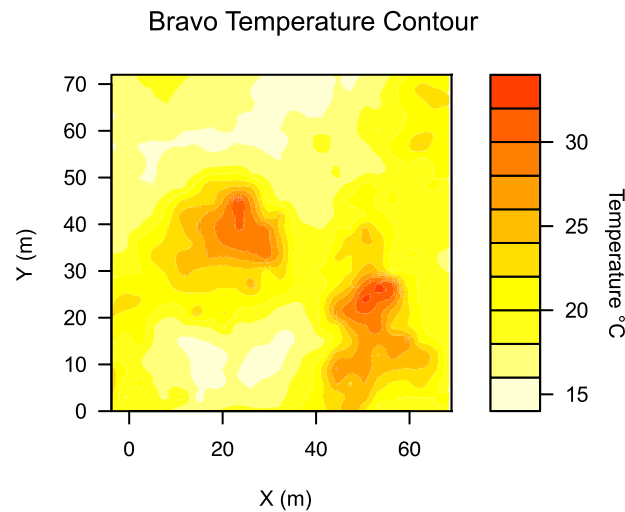
FIGURE 2.4: Contour map of shallow ground temperatures around Bravo hot spring

best fit model was a spherical model but the parameters were quite different – a nugget of 2.5, a sill of 13, and range of 12 meters (Figure 2.5). The parameters from the model variogram were applied to the interpolation of heat flux values with a spacing of 0.50 meters. The resulting contour map of predicted heat flux values is presented in Figure 2.6.

The predicted values were summed and multiplied by the area of each square of the contour grid as given in the following equation:

$$\sum_{n=1}^{\infty} q \times A = P, \tag{2.19}$$

where q equals the conductive heat flux in W/m^2, A equals the area of each grid block on the contour map in m^2, and P is power in watts generated by the conductive heat flux across the 72 x 72 meter grid around Bravo hot spring. Solving this equation gives a total of approximately 13,000 watts. The average flux across the area was 2.39 W/m^2 with a maximum flux of 16.94 W/m^2.

Omnidirectional Semivariogram Bravo Conductive Flux
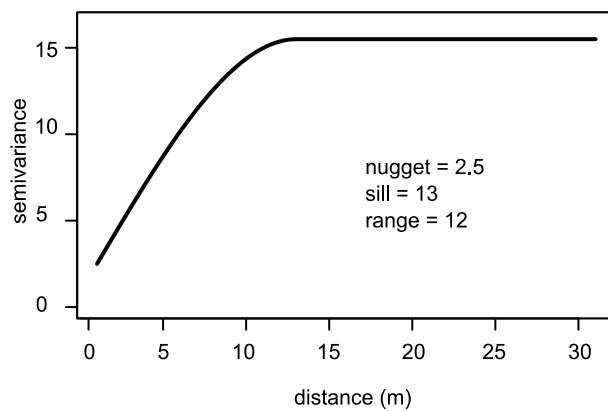
FIGURE 2.5: Omnidirectional sermivariogram of conductive heat flux values around Bravo hot spring

Bravo Conductive Heat Flux Contour
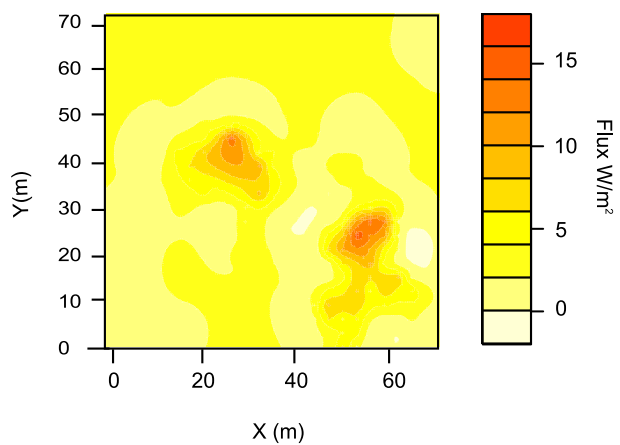
FIGURE 2.6: Contour map of conductive heat flux around Bravo hot spring

2.6 Discussion

Evaluation of the power output by conductive heat flux near Bravo hot springs, as it compares to the advective heat flux from the hot spring itself, indicates that conductive heat flux is not a trivial portion of the total heat output. McMillan et al. (2016) used a deuterium doping method to calculate the volume and subsequent advective output of Bravo hot spring and suggested an output of 18,900 watts. Combined with the conductive output, that is a total 31,900, 41% of which is a product of conductive heat flux.

In the Vaughan et al. (2012) study, researchers used thermal infrared data to capture radiative heat flux in the caldera. The values proffered by Vaughn for the Morning Mist Springs area are consistent with the mean and maximum values calculated in this study. Suggesting the method given here is a reasonable solution for calculating surface heat flux in areas of the caldera with only moderate surface heat flux.

2.7 Conclusions and Future Work

In this study, I have presented a dimensional analysis method for calculating conductive heat flux from the ground in geothermal systems. The necessary data for the analysis were readily collected with minimal invasion and a relatively modest budget. The results align well with the work of others in the Yellowstone Caldera (e.g., Vaughan et al., 2012) but it is clear that more work is needed to get a true balance of heat in the caldera. There are ways the results of this study could be improved and expanded upon:

1. a more thorough analysis of sensitivity and errors of the calculations,

2. multi-directional spatial analysis of the temperature and flux data; and

3. comparison of calculations from other sites (currently we have temperature data for two other locations in the Yellowstone Caldera).

Chapter 3

FLOW PATH INTERACTION IN HYDROTHERMAL AREAS IN LOWER GEYSER BASIN, YELLOWSTONE CALDERA, WY

3.1 Abstract

We present an analysis of flow path connectivity in the Pocket Basin of Lower Geyser Basin, Yellowstone National Park using cluster analysis, a multivariate statistical model. Data used for the cluster analysis include aqueous samples from eleven hot springs and physical parameters collected in the field such as pH and temperature. The cluster analysis indicates a range of well to poorly interconnected near-surface fluid flow pathways and allows for further interpretation beyond standard aqueous geochemical tools such as Stiff and ternary diagrams. This initial, favorable result suggests the method may be useful in the assessment of fluid flow in geothermal systems within a wider range of contexts.

3.2 Introduction

The question of connectivity between subsurface flow paths is an outstanding question in subsurface hydrology. The answer is particularly important in systems where high permeability flow paths discharge at the land surface as connectivity controls the partitioning of flux between pathways and geochemical compositions. For example, Rowland et al. (2008) investigated connectivity between springs separated by tens of meters along a branch of the Hayward Fault near San Jose, California, using geochemical data. On the basis of δ^{18}O and chloride measurements, the investigators inferred limited mixing of waters and low incidence of connectivity between springs in the fracture network. In contrast to the findings of Rowland et al. (2008), Fairley and Nicholson (2006) found strong evidence for mixing in geothermal springs discharging along a portion of the Borax Lake fault zone in the Alvord Basin of southeast Oregon. In that case, the investigators noted only small variations in cation concentrations between 39 springs, and concluded that these slight variations were a result of minor influence of surface

water influx from nearby Borax Lake. A literature review of hydrothermal springs indicates that approximately 78% of springs are associated with known or mapped faults (Curewitz and Karson, 1997), and there is general agreement that faults and fracture zones control hydrothermal fluid flow in the subsurface (Faulds et al., 2006); however, as should be clear from the findings of the Rowland et al. (2008) and Fairley and Nicholson (2006), more work needs to be done to understand the controls, structural and otherwise, on fluid flow within individual fields.

Fluid flow pathways in geothermal systems are hosts to ore deposits (Brown and Simmons, 2003; Micklethwaite and Cox, 2004) and concentrations of rare earth elements (Wood, 2005). Flow path connectivity, to an even greater extent than permeability, controls the economics of fluid extraction for hydrothermal power generation (Tester et al., 2006). Additional work understanding fluid flow networks, at higher resolution, could therefore potentially result in reduced costs associated with mining or extracting ores and metals and more effective exploration and exploitation of hydrothermal systems for energy production.

Since 2014, our research group has worked in the Yellowstone caldera to understand the processes of heat and mass transport associated with hydrothermal springs on the scale of 10s to 100s of meters. The Yellowstone caldera is closed to geothermal development and/or mineral exploration, and therefore offers a pristine natural laboratory for studying geothermal systems. Using data collected from a multidisciplinary approach that included seismic refraction surveys, aqueous geochemical sampling, shallow sub-surface temperature surveys, and meteorological data collection, we have worked to constrain heat flux and characterize fluid flow in the near field vicinity of hydrothermal springs (Lubenow et al., 2016; Price, Lindsey, and Jerry P. Fairley, 2017; N. McMillan et al., 2018). Here, we present a multivariate statistical analysis of geochemical and temperature data, from which we infer the distribution of subsurface flow paths and connectivity between springs in a portion of the Pocket Basin of Lower Geyser Basin, Yellowstone National Park, Wyoming, and corroborate our findings by comparing the results with those from tested and well-known methods for the analysis of aqueous geochemistry of geothermal systems.

3.3 Site Description

Pocket Basin is in the Lower Geyser Basin of the Yellowstone caldera (Figure 3.1). Lower Geyser Basin is the largest hydrothermal area in Yellowstone National Park and includes hundreds of thermal features, including geysers, hot springs, and mud pots. More hot water is discharged in the Lower Geyser Basin than any other area of the caldera (Marler, 1964). Springs in Lower Geyser Basin, in common with springs in nearby geyser basins, are unusual in that they discharge neutral chloride waters as opposed to sulfate rich discharge of areas such as Norris Geyser Basin, Mud Volcano, and similar regions. Surficial sediments in the Lower Geyser Basin are dominated by glacial and alluvial sediments, as well as deposits of sinter, silica mud, and minor travertine that have precipitated from the thermal discharge (L.J. Muffler et al., 1982). The basin is surrounded by rhyolitic plateaus ranging from 120 to 300 meters above the basin floor with ages of the flows ranging from 120,000 to 600,000 years (L.J.P. Muffler, D.E. White, and A. Truesdell, 1971). Alignment of thermal features in Lower Geyser Basin implies generally northwest trending lineations which are overprinted by the southwest trend of the Lava Creek contact from Nez Perce Creek to Twin Buttes where Pocket Basin lies (L.J.P. Muffler, D.E. White, and A. Truesdell, 1971).

Pocket Basin is an oval-shaped depression approximately 400 meters by 900 meters, and is one of several hydrothermal explosion craters located in the caldera (L.J.P. Muffler, D.E. White, and A. Truesdell, 1971). Hydrothermal explosion craters are the result of subsurface fluid pressure exceeding the overlying rock tensile strength plus the lithostatic load (Nelson and Giles, 1985). In the case of Pocket Basin, melting of the glaciers at the end of the Pinedale Glaciation is hypothesized to have reduced the lithostatic load. The resulting boiling and increase in subsurface fluid pressure triggered a hydrothermal eruption and ejected debris across the surrounding area (L.J.P. Muffler, D.E. White, and A. Truesdell, 1971). The geologic map of the Lower Geyser Basin identifies the near surface materials as consisting of white to light brownish gray diatomacious silt deposited in the flat marshy areas near the hot springs; away from thermal springs, surficial deposits include hydrothermal explosion debris and moderately to well sorted sands and gravels interpreted as outwash from the Pinedale Glaciation (L.J. Muffler
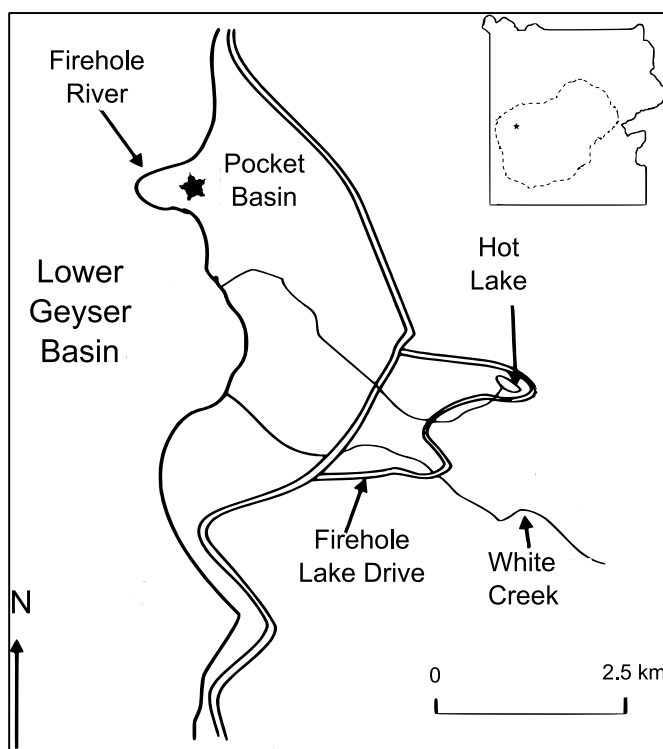
FIGURE 3.1: Map of Lower Geyser Basin (LGB) study area, with Pocket Basin field area marked by star. Inset map (upper right) shows the Yellowstone National Park boundary (bold outline) and the Yellowstone caldera (dashed line); small star on inset indicates approximate location of the LGB detail map.

et al., 1982). Field relationships presented by Christiansen et al. (2007) constrain the time of the hydrothermal explosion to the end of the last glacial period approximately 16,000 years before present. Pocket Basin has over 50 thermal features situated along the Firehole River (Rodman and Guiles, 2008), most of which are circum-neutral chloride rich springs depositing silicious sinter. Much of the area is marshy and difficult to traverse. The focus area for this study was located in the southeastern quadrant of the basin, situated near the crater rim, and slightly above the marshy flats.

3.4 Methods

3.4.1 Sampling Methods

We collected aqueous samples from eleven springs located along the Firehole River in Pocket Basin. These samples were obtained from the center of each spring at approximately half of the water depth using a 2 centimeter diameter by 1.5 meter long polyethylene Zurn Pex pipe with a single-hole rubber stopper inserted at one end. The samples were filtered immediately into a Fisherbrand 15 milliliter centrifuge tube using a Luer lock syringe equipped with a 0.45-micron filter. Cation samples were preserved with 10% nitric acid to prevent precipitation. Both anion and cation samples were sealed with parafilm to protect against atmospheric contamination and loss of fluids. Samples were transported on ice in a cooler until analysis to avoid exposure to light and to discourage mineral precipitation. We also collected *in situ* pH, temperature, and electrical conductivity measurements using a Vernier LabQuest handheld data logger on all 11 springs.

3.4.2 Ground Temperature Measurements

Shallow subsurface temperatures were collected on a 15 x 50 meter grid enclosing all springs except 109. Spring 109 is just to the west of the collection grid on a small area raised slightly above the surroundings. There is a northwest-southeast striking linear feature along the western edge the collection grid, which we interpreted as possibly indicating a near-surface fracture. We used 20 centimeter Omega Rugged Penetration Thermocouple Probe (K-type) with a "T" handle connected to Fluke 51 II single input digital thermometers with a reported accuracy of $\pm 0.05\% + 0.3$ ° to record temperatures at 1.5 meter intervals. Methods for temperature collection can be found in greater detail in Lubenow et al. (2016). We performed geostatistical analysis of the temperatures and used the resulting temperature estimates to create a temperature contour map of the area, as can be seen in Figure 3.4.

3.4.3 Analytical Methods

Within 5 hours of collection, we obtained total alkalinity (TA) by titrating each sample with sulfuric acid to an end point of pH 4.5. In hindsight, the authors recognize that the inflection point method is the preferred method for calculating total alkalinity; therefore, samples with a cooled pH below 4.5 show a total alkalinity of 0 which we know to be untrue since the warm pH ranged from 5.52 to 7.95. Bicarbonate concentrations were back-calculated using the equation (Snoeyink and Jenkins, 1980):

$$TA = \frac{mL(H_2SO_4) * 0.02\frac{eq}{L} * 50,000\frac{mg(CaCO_3)}{eq}}{50mL(Sample)}. \tag{3.1}$$

Cation concentrations were determined by the University of Idaho Soil Science Laboratory using a ThermoFisher iCAP 6300 inductively coupled plasma atomic emission spectrometer (ICP-AES). Anion samples were analyzed at the University of Idaho Analytical Sciences Laboratory using a Dionex DX-100 ion chromatograph with a suppressed ion conductivity detector.

3.4.4 Data Preparation

For the present study, we expected to apply statistical clustering to the analysis of our data. The results of cluster analysis can be affected by missing data values; therefore, the handling of species concentrations below detection must be carefully considered. In statistical terminology, the removal of data points occurring below the measurement range of the equipment is known as left truncation (Pickering, Bull, and Sanderson, 1995). To adjust for this truncation, we use the VanTrump and Miesch method (VanTrump and Miesch, 1977; Güler, Thyne, and McCray, 2002), which replaces concentrations below the detection limit with 3/4 of the detection limit or above the saturation limit of the equipment with 4/3 the limit. Three of the 23 species concentrations measured (bromide, zinc, and iron) required correction for at least some samples collected. Species for which 50% of the values were either above or below the detection limit (nitrate, nitrite, phosphate, copper) were omitted from this study.

In order to apply cluster analysis to data sets in which the magnitude of the individual variables may differ dramatically, it is necessary to scale the data. Several methods exist to scale data, and much debate centers around the best method (Souto et al., 2008; Mohamad and Usman, 2013). We chose to analyze our data as normalized z-scores. The objective of the z-scores is to rescale a dataset such that the mean is 0 and the standard deviation is 1 using the formula:

$$z = \frac{x - \bar{x}}{s_x},$$
(3.2)

where x is the variable to be transformed, $\bar{x}$ is the sample mean, s_x is the sample standard deviation, and z is the transformed variable. Performing cluster analysis on z-score normalized variables rather than on non-normalized, min-max normalized, or decimal-scaled normalized variables has been shown to provide more accurate clustering (Mohamad and Usman, 2013).

3.4.5 Clustering Methods

Cluster analysis has applications in a wide range of disciplines such as biology (Jiang, Tang, and Zhang, 2004), psychology (Clatworthy et al., 2005), and marketing (Punj and Stewart, 1983). The method is currently underutilized in the earth sciences, although there is evidence that this may be changing (Güler, Thyne, and McCray, 2002; Mayer et al., 2014; Lindsey et al., 2018). While cluster analysis has been used in previous studies of geothermal fluids (Veldeman et al., 1990; Irawan et al., 2009), these studies have focused on characterizing hydrogeological systems over many kilometers as opposed to characterizing flow on a fine-scale. Veldeman used cluster analysis along with correspondence factor analysis to differentiate thermal waters over 10s to 100s of kilometers. The cluster analysis successfully created two clusters - one of low temperature, high TDS waters and the other a higher temperature, mineralized water. Irawan et al. (2009) applied cluster analysis to a volcanic hydrothermal system in Indonesia and used the results to divide the fluids into three distinct hydrogeological systems of origin.

Cluster analysis is a multivariate statistical method for finding groups within data. Grouping is accomplished by dividing data into "clusters" which have the most similarity within the cluster and most difference between clusters (Tan, Steinbach, and Kumar, 2006). The between

and within cluster sum-of-squares is often used to measure this difference and/or similarity. Cluster analysis algorithms are generally aimed at finding efficient, near-optimal solutions to the problem of grouping large numbers of items, and many programs exist to perform cluster analysis quickly and easily once the data have been formated correctly. For our analyses we use the statistical computing environment R (R Core Team, 2014).

Two types of clustering are used for this analysis. The first, hierarchal clustering, does not require the investigator to assign a number of clusters. We use this method as a basis for defining cluster numbers for the k-means cluster analysis discussed below. For this analysis, we use the complete-linkage method, often referred to as the furthest neighbor method. Complete-linkage uses the distance between the most remote objects to create the groups. At each step of clustering, the maximum distance is found for all clusters, and the two clusters with the smallest distance are merged. Once a k-value is chosen based upon the hierarchal cluster, k-means clustering is completed.

The final cluster model, k-means clustering, partitions data based upon some chosen numeric criterion. In this case, as in most cases, the numeric criterion used is the within sum-of-squares. A more thorough review of our clustering techniques can be found in Lindsey et al. (2018); also see Everett (1980; 2010) and Anderberg (2014).

3.5   Results

3.5.1   Geochemical Analysis

Results of the geochemical analyses are presented in Tables 3.1, 3.3, and 3.2. Table 3.1 includes field parameters collected for each spring – pH, temperature, and electrical conductivity. Table 3.2 reports anion concentrations and Table 3.3 reports cation concentrations, both in mg/L. Major ion concentrations are presented graphically in Figure 3.2 as Stiff diagrams to allow visual comparison of the spring compositions. Sulfate, chloride, and bicarbonate are plotted on a ternary diagram provided in Figure 3.5.
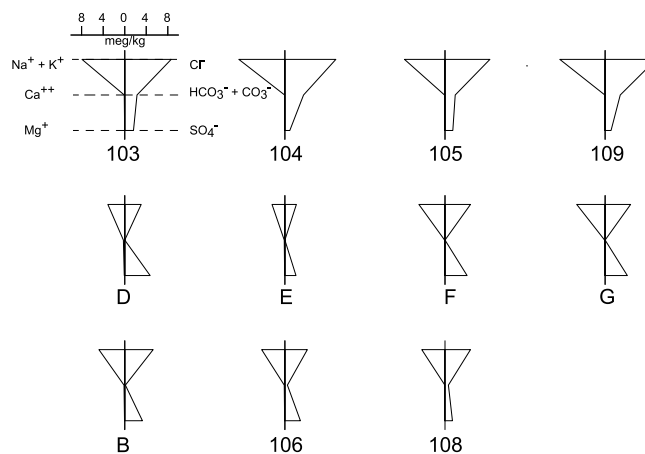
FIGURE 3.2: Stiff diagrams for all springs.

TABLE 3.1: Physical parameters collected in situ.

Spring #	pH	EC (microS)	Temp (Celcius)
103	8.4	1277	70.3
104	8.65	1414	65.7
105	7.65	1211	85.6
108	5.95	658	91.6
109	9.57	1384	65.1
B	8.23	832	55.1
106	8.84	733	59.9
D	7.95	840	52.7
E	4.84	373	93.8
F	6.53	847	69.5
G	5.52	854	66.7

TABLE 3.2: Anion concentrations reported in mg/L.

Spring #	Br	Cl	F	SO3	HCO3
103	0.95	310	28	79	140.65
104	0.97	340	31	45	214.96
105	0.88	300	27	71	117.35
108	0.47	70	18	67	39.81
109	0.99	340	30	53	174.05
B	0.54	190	16	160	7.78
106	0.43	150	15	140	29.4
D	0.41	110	13	230	0
E	ND	77	8.9	100	0
F	0.82	170	13	200	0
G	0.42	170	13	200	0

TABLE 3.3: Cation concentrations reported in mg/L.

Spring #	As	B	Ca	Fe	K	Li	Mg	Mn	Na	Pb	Si	Zn
103	1.389	3.939	1.652	bdl	11.74	3.546	9.564E-2	1.790E-2	177.9	7.51E-2	120.1	4.90E-3
104	1.399	4.353	1.028	bdl	9.902	4.004	8.500E-3	2.400E-3	193.6	7.280E-2	117.6	2.70E-3
105	1.185	3.767	1.666	bdl	11.6	3.398	9.800E-2	1.67E-2	168.5	7.31E-2	117.1	bdl
108	0.566	2.127	0.501	bdl	7.25	1.767	2.100E-2	8.30E-3	96.23	7.40E-2	116.8	2.4E-2
109	1.357	4.194	1.178	1.44E-2	10.12	3.755	4.3E-3	1.60E-3	190.1	7.00E-2	111.4	8.0E-3
B	0.544	2.31	2.71	9.89E-2	15.86	1.969	0.5386	7.66E-2	102.6	7.93E-2	124.7	2.32E-2
106	0.516	2.038	2.496	0.850	14.28	1.733	0.4744	6.85E-2	91.76	7.72E-2	119.7	3.16E-2
D	0.558	1.436	5.168	14.07	14.29	1.097	1.1040	0.162	64.72	7.39E-2	113.6	6.69E-2
E	0.440	0.940	2.414	0.538	9.22	0.827	0.4834	7.27E-2	50.33	9.71E-2	159.8	6.75E-2
F	1.098	2.218	1.629	4.11E-2	11.48	2.008	0.1568	3.39E-2	106.2	8.57E-2	137.4	2.85E-2
G	1.061	2.262	2.037	2.96E-2	13.17	2.16	0.1882	3.92E-2	115.1	8.61E-2	138.1	0.307

3.5.2   Ground Temperatures

More than 350 shallow-subsurface temperatures were recorded over the 15 meter x 50 meter field area. To identify the spatial correlation structure of the temperature data, we developed both directional and omnidirectional variograms. Initially, directional variograms were plotted at 0, 45, 90, and 135 degrees to identify anisotropy. The directional variograms did not show evidence of significant anisotropy in the temperature correlation structure; as a result, we concluded the spatial correlation was adequately modeled by an isotropic (i.e., omnidirectional) model variogram. We used a isotropic spherical model model with a nugget of 2.13, a sill of 2.82, and a range of 14.89 meters (Figure 3.3). For further information regarding development of this method, see Fairley et al. (2003) and others (e.g., Heffner and J. Fairley, 2006; Anderson and Jerry P. Fairley, 2008; Lubenow et al., 2016). The model variogram was used to interpolate temperatures on a 1.25 meter scale using kriging, a geostatistical interpolation method, and a contour of the temperatures was plotted (Figure 3.4).

3.5.3   Hierarchal Clustering

The results of the complete linkage method can be seen in Figure 3.6. We read the dendrogram from top to bottom. Each vertical line in the dendrogram is a clade and represents a grouping with multiple members. Single lines of the dendrogram are leaves. The dendrogram shown in Figure 3.6 has 2 majors: clade 1 includes 9 springs (109, 104, 103, 105, F, G, 108, 106, and B) while clade 2 has only 2 springs (D and E). Clade 1 continues to subdivide, before ending with the smallest clades (clusters), each containing no more than 2 members. To determine
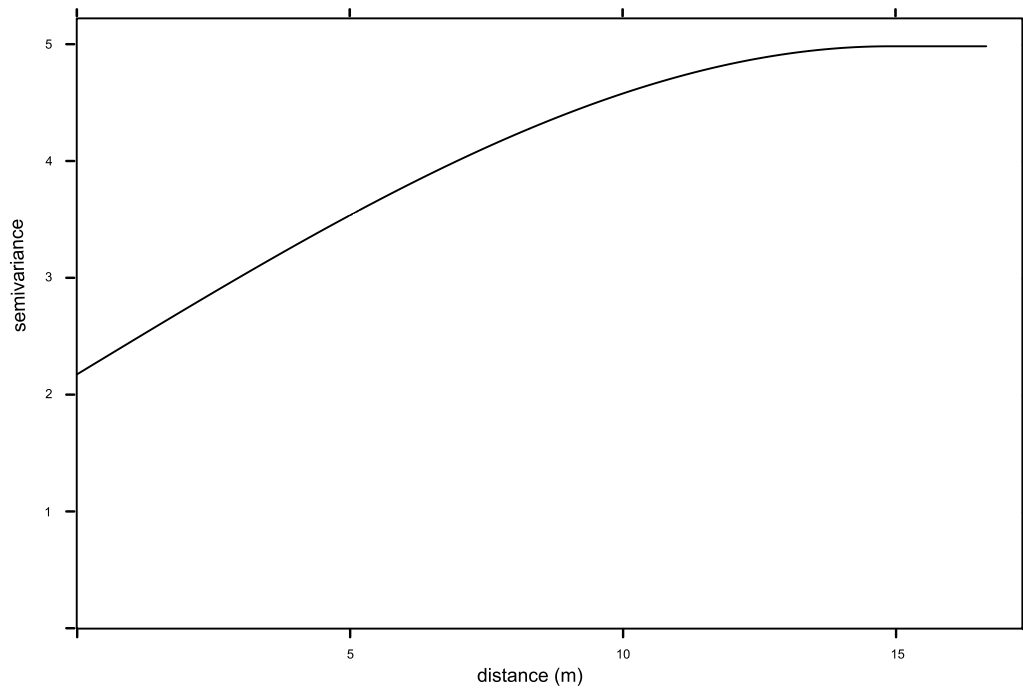
FIGURE 3.3: Variogram of ground temperatures at Pocket Basin.
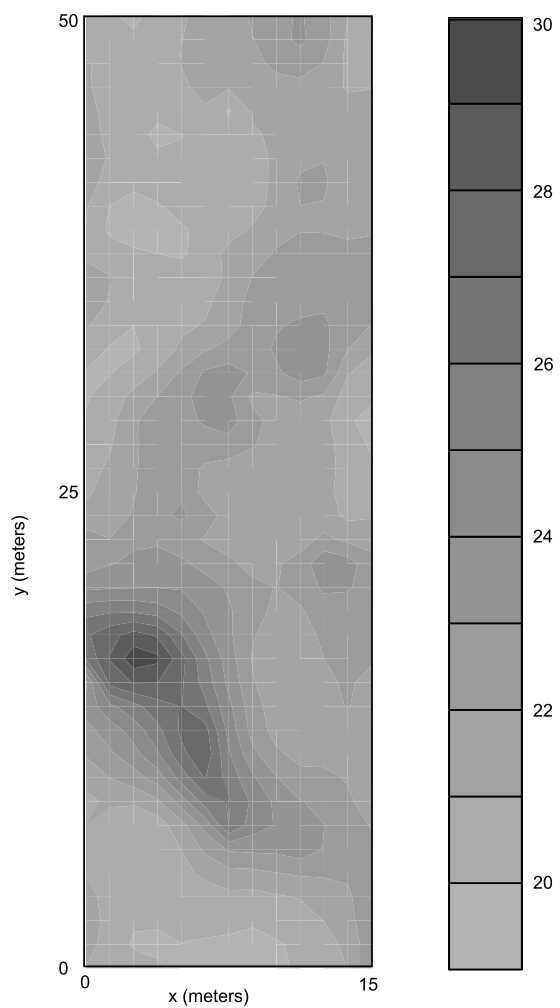
FIGURE 3.4: Kriged ground temperature contour of Pocket Basin field area.
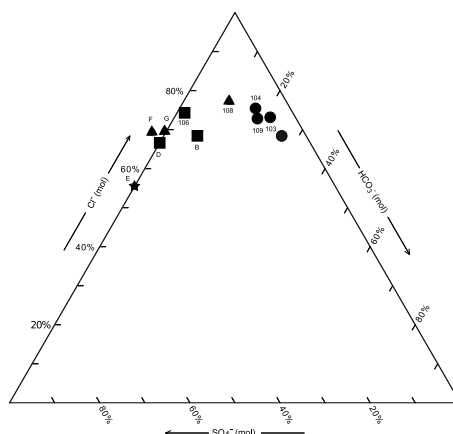
FIGURE 3.5: Ternary diagram for all springs.

the best number of clusters (k) moving forward for the k-means clustering, we look for these major divisions. A review of the dendrogram demonstrates the value of k for the Pocket Basin dataset should lie between 2 (the first major division) and 7 (the final number of divisions). Grouping of the data into 7 clusters is unlikely to provide much information on between-spring relationships, given the small number of objects (11 springs) in the dataset. Visual inspection of the dendrogram in Figure 3.6 provides support for the idea of three major clades (i.e., clades 2, 3, and 4), which comprise springs D and E (clade 2), springs 109, 104, 103, and 105 (clade 3), and spring F, G, 108, 106, and B (clade 4). We therefore provisionally identified a value of k=3 as offering an optimal value for the k-means cluster analysis, while evaluating values of k=2, 3, 4, 5 as a sensitivity analysis to refine this choice as described in the following Section 4.4.

3.5.4   K Means Clustering

After completion of the hierarchal cluster, we proceed with k-means clustering with values of k from 2 to 5. In addition to the fact that the dendrogram indicated a k between 2 and 7, we calculated the change in within sum-of-squares for k = 2, 3, 4, & 5. The change in the sum-of-squares ratio is less than 10% from 4 to 5 and is an appropriate threshold for this small data set.
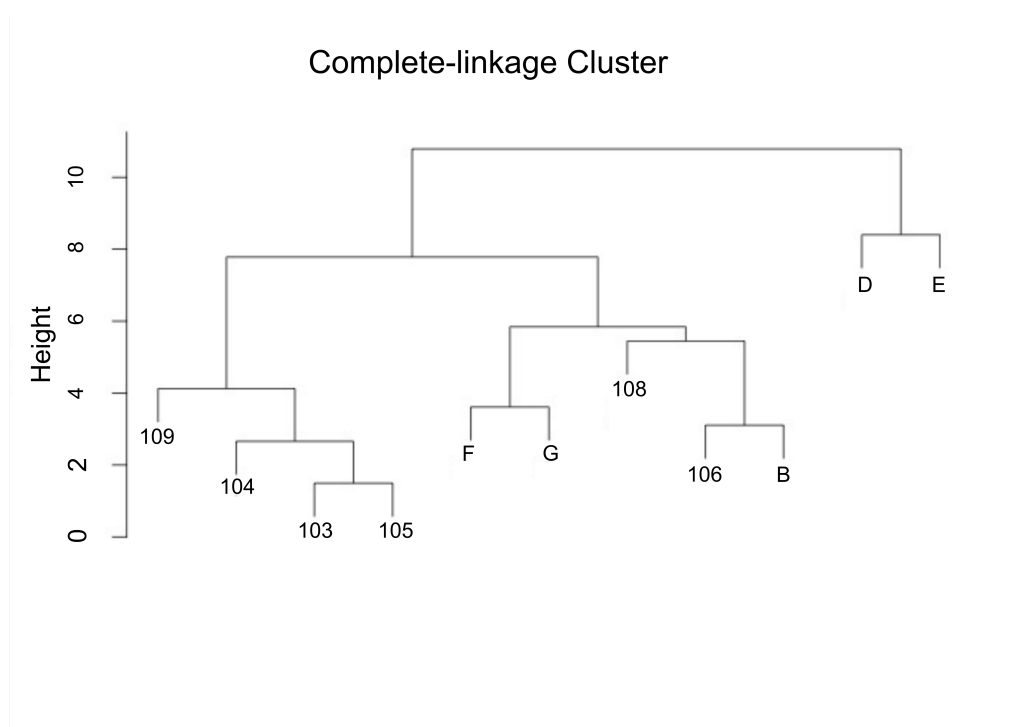
FIGURE 3.6: Hierarchal Cluster dendrogram complete-linkage method.

TABLE 3.4: Change in sum of square ratio by cluster number.

Clusters	SSB/SST
2	42.4%
3	58.4%
4	72.1%
5	79.5%

TABLE 3.5: k-means cluster members

Spring	Cluster
103	1
104	1
105	1
109	1
B	2
D	2
106	2
E	3
F	4
G	4
108	4

The values can be seen in Table 3.4. The small change in percentage supports a k value of 4. The final membership of each cluster can be seen in Table 3.5.

3.6 Discussion

Given the small spatial extent of the study area, it seems reasonable to assume that discharge for all the springs in the study area originates from the same source. Boron, chloride, and lithium ratios are often used as an indication that samples share (or do not share) a common origin; in this case, the consistency of the B/Li ratios (1.1 ± 0.07) and Cl/B (78.5 ± 2.8) support the assumption that all springs are from the same source (K. Nicholson, 1993). The average Na/K ratio is 11.1 ± 5. In general, Na/K ratios of < 15 indicate rapid ascent to the surface as well as association with up-flow structures and high permeability zones (K. Nicholson, 1993). All ratios can be found in Table 3.6. These observations provide our first two inferences about

TABLE 3.6: Geochemical Ratios

Spring ID	Cl/B	Cl/Li	Cl/As	Na/K	B/Li	Na/Ca
103	78.70	87.42	223.18	15.15	1.11	107.69
104	78.11	84.89	243.03	19.55	1.09	188.33
105	79.64	88.29	253.16	14.53	1.11	101.14
106	73.60	86.56	291.04	6.43	1.18	36.76
108	79.92	96.21	300.25	13.28	1.20	192.08
109	81.07	90.55	250.55	18.78	1.12	161.38
B	82.25	96.50	349.20	6.47	1.17	37.86
D	76.60	100.27	197.03	4.53	1.31	12.52
E	81.89	93.06	175.04	5.46	1.14	20.85
F	76.65	84.66	154.83	9.25	1.10	65.19
G	75.15	78.70	160.23	8.74	1.05	56.50
mean	78.51	89.74	236.14	11.11	1.14	89.12
sd	2.79	6.32	61.85	5.39	0.07	66.09

the shared characteristics of the flow paths for all the springs in our study: discharge originates from one source, and ascends rapidly along high-permeability pathways to the surface. Beyond these observations, which apply to all the springs in our study, we can further differentiate shared characteristics that are common to subsets of springs, and give insight into some of the factors responsible for between-spring relationships. In the following, we suggest possible interpretations of the clustering and geochemistry of those subsets.

Cluster 1 contains four springs (103, 104, 105, and 109). Cluster 1 springs have the highest Na/K ratio of all springs in the area, though still below 15, and the highest bicarbonate levels both suggesting increased lateral flow and conductive cooling (K. Nicholson, 1993). Evidence for this is provided by the halos of elevated ground temperatures, visible in Figure 3.7, that surround the springs in this group. The chloride concentrations of these springs (Table 3.2) are close to those inferred for the Yellowstone "parent" geothermal fluid, from which all thermal waters in the caldera are hypothesized to originate (R. O. Fournier, 1989). The relatively high pH (8.4 to 9.57) and moderately high chloride concentrations suggest discharge from these springs has not undergone phase separation or mixing with shallow meteoric water. Furthermore, the low calcium concentrations are indicative of low levels of water-rock interaction. We

interpret this as the geothermal fluids follow a fracture, fault, or contact to the surface, limiting water-rock interaction and at such a rate as to inhibit phase change. Consequently, these springs may be the best representation of the shallow reservoir or mutual flow path shared by all the springs before they diverge in the near-surface. Further review of the ternary diagram with classification fields added (Figure 3.8) shows springs 103, 104, 105, and 109 plotting near the chloride apex, indicating these are relatively mature geothermal waters, with compositions indicative of deep origin, similar to the parent fluid of Fournier (1989).

Although the chemistries of the springs in cluster 1 demonstrate clear similarities, there are also differences between the springs in this group. The dendrogram (Figure 3.6) indicates this clade can be subdivided into smaller clusters, with springs 103 and 105 in one sub-group, and springs 104 and 109 in the other sub-group. The subdivisions of cluster 1 are apparently the result of minor differences in aqueous chemistry; as can be seen in the Stiff diagrams (Figure 3.2), springs 104 and 109 show slightly elevated carbonate levels, while springs 103 and 105 display somewhat higher sulfate. The two sub-groups of clade 1 present different physical aspects in the field, as well: in keeping with their higher temperatures, springs 104 and 109 display mats of orange cyanobacteria, have low turbidity, and display water surfaces that are flush with the surrounding ground surface. In contrast, springs 105 and 103 demonstrate higher turbidity, well-developed communities of green and blue-green cyanobacteria, and have water levels that are recessed below the nearby land surface (Figure 3.9).

Cluster 2 contains springs B, D, and 106. These springs show high levels of water-rock interaction as supported by relatively low Na/K ratios and increased levels of some cations such as magnesium and calcium; however, they do not appear to have experienced phase change as indicated by the higher pH. The water-rock interaction here is likely a function of travel distance/time and is evidenced by high magnesium, calcium, and potassium as well as low chloride and boron.

Cluster 3 is populated by a single spring (spring E), which has the highest temperature (93.8 °C) and lowest pH (4.84) of the springs in our study area (Table 3.1). The high temperature and moderately low pH are suggestive of a certain amount of phase separation in the near-surface;
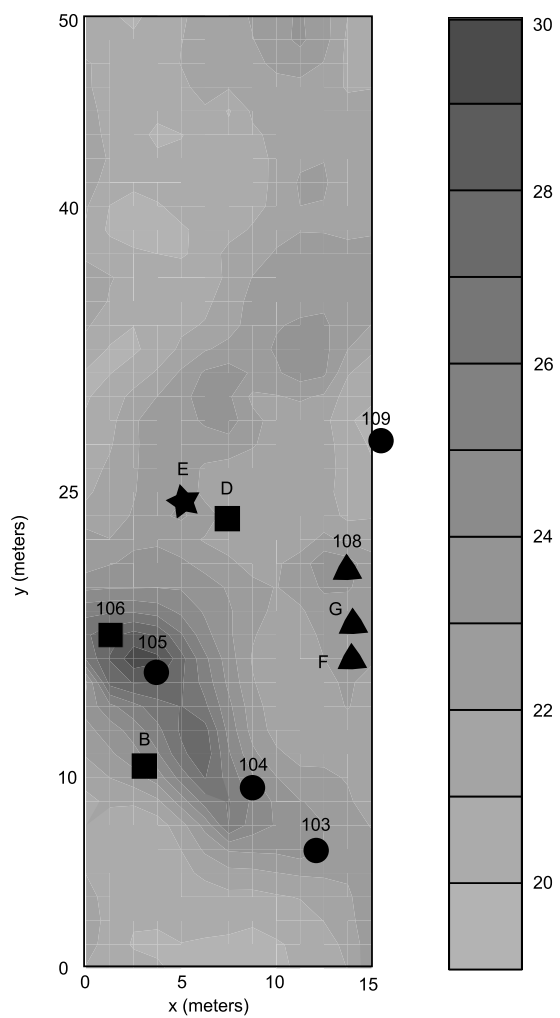
FIGURE 3.7: Shallow subsurface temperature grid with cluster overlay.
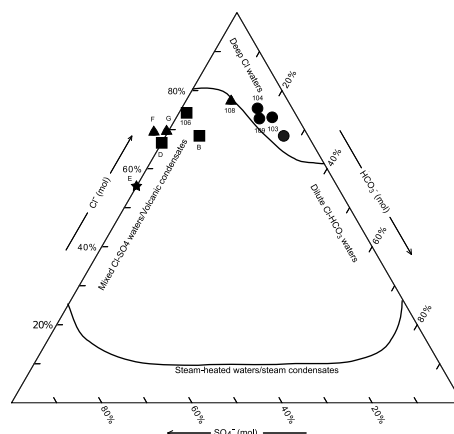
FIGURE 3.8: Ternary diagram of all springs with classification fields included.

during phase separation, H_2S partitions to the vapor phase and oxidizes to sulfuric acid, which condenses with the vapor in the near-surface. This process is discussed in depth in Truesdell & Nathenson. (where similar behavior was seen in the Shoshone Basin of Yellowstone National Park. The probability that discharge from spring E contains a significant fraction of condensed vapor is further supported by the relatively low chloride concentration (77 mg/L) and below-detection levels of bicarbonate. Spring E plots closer to the steam heated/condensate field (although not within the field) than any other spring in this study area, and the elevated levels of calcium, magnesium, and silica likely derive from high levels of interaction between geologic materials and relatively low pH condensate in the near-surface.

Cluster 4 contains springs F, G, and 108. These three springs are located along a linear feature that was observed in the field, and which is also associated with a linear temperature anomaly visible in the temperature data (Figure 7). This feature generally strikes northwest to southeast, and is hypothesized to be the expression of a discontinuity in the bedrock (e.g., a fault, joint, or zone of fracturing). The chemistries of the springs in this group suggest moderate water-rock interaction (calcium, sodium, potassium, and magnesium) and show little evidence for phase separation or mixing with low pH condensate. However, the moderate (F, G) to low (108)
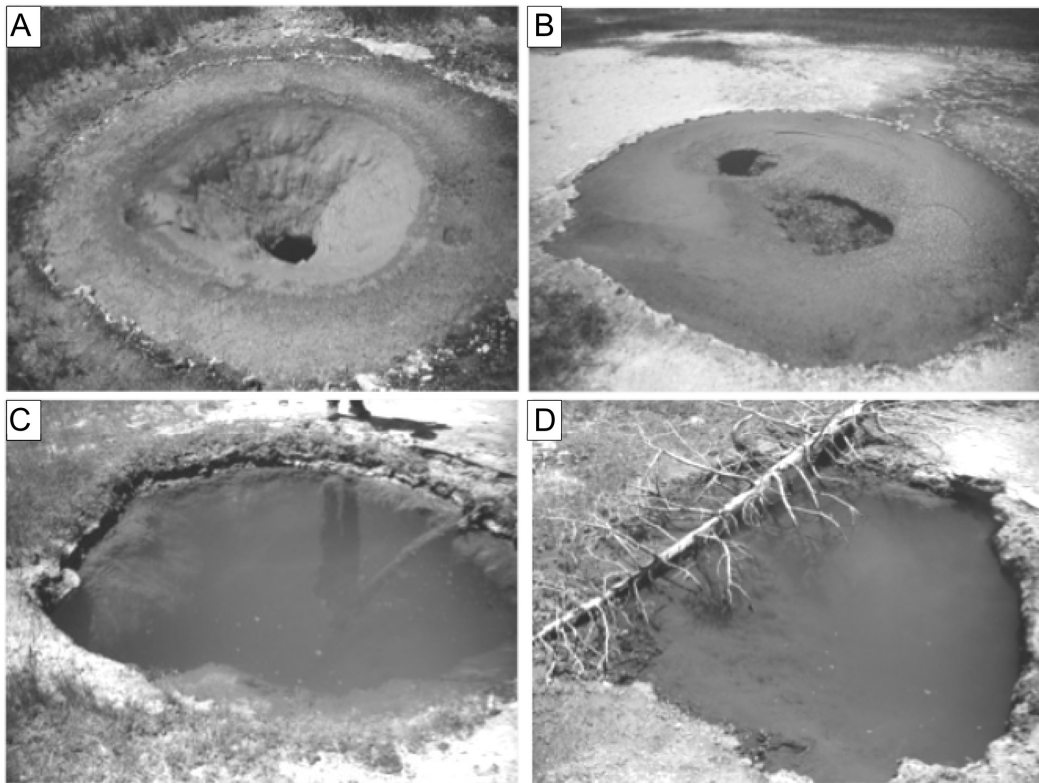
FIGURE 3.9: The four largest springs in the study. A. Spring 104, B. Spring 109, C. Spring 103, and D. Spring 105.

chloride and moderate dissolved load (as inferred from electrical conductivity measurements, see Table 1) suggest possible mixing with near-surface meteoric waters. We hypothesize that the linear feature along which these springs are aligned constitutes a permeable pathway for rising hydrothermal fluids, while facilitating mixing with surface waters that migrate along the open fractures from the marshy wetland areas adjacent to the western margin of the study area. As a result of the small size of the study area and close proximity of the springs, the differences in the observed chemistries are slight. In most respects, the assignments of springs to the various clades by cluster analysis do not differ from groupings that might be made on the basis of standard methods of geochemical analysis (e.g., ternary diagrams, Piper or Stiff plots, etc.). Of particular interest, however, is the classification of spring 108 into cluster 4. On the basis of the ternary diagram (Figure 3.5) and geochemical ratios (particularly the elevated Na/Ca ratio; Table 3.6), spring 108 is most similar to springs 103, 104, 105, and 109, and would likely be placed with them in cluster 1. The cluster analysis, however, differentiates between the springs of cluster 1 and spring 108, placing it instead with springs F and G in cluster 4. This is likely due to the pH (5.95), which fits better with springs F and G than the slightly alkaline springs of cluster 1, and possibly as a result of the lower concentrations of some anions (chloride, fluoride, bromide, bicarbonate), and cations such as sodium and lithium, in comparison to cluster 1. The close proximity of these three springs (F, G, and 108), and their alignment along the linear feature described above, is a persuasive argument that the cluster analysis correctly binned these springs together. The cluster analysis therefore, picked out a subtle, but potentially valuable, relationship that might have been lost or overlooked on the basis of the standard graphical analyses used to interpret geochemical data. Thus, although the majority of information that can be obtained from cluster analysis is similar to that delivered by more common methods, cluster analysis offers the potential to uncover additional, valuable insights into data relationships that might otherwise go unnoticed.

The results of the cluster analysis and the graphical methods for interpreting aqueous geochemistry data for the Pocket Basin springs has important implications for using geochemistry to infer connectivity between springs located in hydrothermal discharge areas. As already

noted, the small size of our study area (approximately 75 m^2) makes it unlikely that discharge originates from more than one source, with the possible exception of minor mixing from surface waters inferred for springs F, G, and 108. Even so, variations in spring chemistry arising from near-surface water-rock interaction and vapor separation, probably related to differences in flow path permeability and the composition of surficial geological materials encountered, are sufficient to register in both graphical and cluster analyses. The logical conclusion is therefore that heterogeneous geochemistry may not always be a reliable indicator of flow path isolation between springs; likewise, homogeneous chemistry may not indicate flow path connectivity. For example, Fairley and Nicholson (2006) inferred highly interconnected and well-mixed flow within the Borax Lake fault in southeast Oregon, on the basis of largely homogeneous chemistry from 175 springs sampled along the 800 m fault trace. Although the geological and hydrological setting of the Borax Lake fault do support a high degree of communication between flow paths and a single source for the geothermal fluids (with the exception of minor mixing with shallow interflow from nearby Borax Lake; Fairley and Nicholson (2006), it may be said that the real implication of the homogeneous chemistry is that the sampled fluids encountered similar geology and conditions in the near-surface. In contrast to the findings of Fairley and Nicholson (2006), Rowland et al. (2008) found evidence for substantially isolated flow in pathways feeding 13 springs at Alum Rock State Park, distributed over a distance of about 300 meters along the trace of the Hayward fault near Fremont, California. The Rowland et al. (2008) study primarily relied on chloride concentrations and stable isotopes (deuterium and δ^{18}O) as the basis of their inferences. The conservative nature of chloride, and relatively low temperatures of the springs ($15 \leq T \geq 29$ °C) probably precluded shallow boiling and minimized the influence of near-surface water-rock interaction. Unfortunately, these tracers offer less information than a full suite of major and trace elements, limiting the potential for greater insight into fluid flow paths and subsurface processes.

3.7 Conclusions

In this study, we present data from an investigation of near-surface flow paths of 11 thermal springs, located in the Pocket Basin area of Lower Geyser Basin, Yellowstone National Park. The spring data includes water, pH, temperature, and major- and trace-element concentrations; in addition, we obtained shallow ground temperature data (20 cm depth) for an area of approximately 75 m^2 (i.e., a 15 x 50 m grid) in the vicinity of the springs, with temperature measurements made at a spacing of 1.5 x 1.5 m. The geochemical and water temperature data were analyzed using standard graphical methods (e.g., Stiff diagrams and ternary diagrams, geochemical ratios, etc.) and the statistical method of cluster analysis to identify relationships between springs, with the objective of identifying near-surface processes (boiling, mixing, etc.) operating in the discharge area, and potentially inferring the extent of connectivity between flow paths. Our analyses indicate there are subtle, but definite, differences between waters discharging from springs even within this small study area, and that the differences are likely due to variations in near-surface conditions and processes such as phase-separation and water-rock interaction. Furthermore, comparison with the ground temperature data implies that the near-surface character of the flow pathways feeding individual springs exerts significant control on spring properties. For example, flow along high-permeability fracture conduits is likely to have limited water-rock interaction, higher discharge temperature, and potentially lower pH as a result of phase separation of mixing with acidic condensate, while flow through lower-permeability porous materials may demonstrate higher pH and greater evidence of water-rock interaction. The extent to which near-surface fractures may connect with and promote mixing between hydrothermal fluids and low-temperature meteoric (surface) water can also have an impact on the observed character of spring discharge. Thus, differences between hydrothermal discharge, even from springs in close proximity, is likely to be a complex function of near-surface geology and mineralogy, fracture network geometry and density, and the initial chemistry of both deep and surface fluids. Although the intricate and nonlinear relationships between these factors complicate attempts to identify simple correlations between springs, they also offer a potentially rich source of information on near-surface processes in hydrothermal

discharge areas.

Apart from any insight that may have been gained on near-surface processes impacting the differentiation of hydrothermal spring discharge, the study presented here illustrates the potential utility of statistical cluster analysis. Although many of the inferences in this study are based on standard methods of geochemical data analysis, cluster analysis appears to offer a robust alternative that can be used in conjunction with standard approaches to seek relationships between samples; in some cases, cluster analysis may highlight connections between samples that could otherwise be overlooks (as with spring 108 in the present study). A wealth of data exists on geothermal systems worldwide; for example, the Yellowstone Research Coordination Network contains a large amount of data for springs in and around the Yellowstone caldera; outside of Yellowstone, the National Geothermal Data System is a bank for data on systems in the United States with geothermal development potential, and similar databases exist for other regions of the world. In many cases the challenge is not to obtain data of interest, but rather to identify relationships of interest within a large number of datasets that contain data that vary widely in quality, granularity, and method of collection. We suggest that statistical cluster analysis is a useful tool for making such comparisons, for small areas (as in this study), and potentially at regional or larger scales (Lindsey et al., 2018).

Bibliography

Anderberg, Michael R. (2014). *Cluster analysis for applications: probability and mathematical statistics: a series of monographs and textbooks*. New York, NY: Academic Press.

Anderson, Todd R. and Jerry P. Fairley (2008). "Relating permeability to the structural setting of a fault-controlled hydrothermal system in southeast Oregon, USA". In: *Journal of Geophysical Research: Solid Earth* 113.B5. B05402, n/a–n/a. ISSN: 2156-2202. DOI: 10.1029/2007JB004962. URL: http://dx.doi.org/10.1029/2007JB004962.

Benseman, R. F. (1959a). "Estimating the total heat output of natural thermal regions". In: *Journal of Geophysical Research* 64.8, pp. 1057–1062. ISSN: 2156-2202. DOI: 10.1029/JZ064i008p01057. URL: http://dx.doi.org/10.1029/JZ064i008p01057.

— (1959b). "The calorimetry of steaming ground in thermal areas". In: *Journal of Geophysical Research* 64.1, pp. 123–126. ISSN: 2156-2202. DOI: 10.1029/JZ064i001p00123. URL: http://dx.doi.org/10.1029/JZ064i001p00123.

Brown, Kevin L. and Stuart F. Simmons (2003). "Precious metals in high-temperature geothermal systems in New Zealand". In: *Geothermics* 32.4, pp. 619–625.

Clatworthy, Jane et al. (2005). "The use and reporting of cluster analysis in health psychology". In: *British Journal of Health Psychology* 10, pp. 329–358.

Dawson, G. B. (1964). "The nature and assessment of heat flow from hydrothermal areas". In: *New Zealand Journal of Geology and Geophysics* 7.1, pp. 155–171. DOI: 10.1080/00288306.1964.10420167. URL: https://doi.org/10.1080/00288306.1964.10420167.

Ellis, A.J. and S.H Wilson (1955). "The heat from the Wairakei- Taupe thermal region calculated from the chloride output". In: *New Zealand Journal of Science and Technology* 36 (6), pp. 622–631.

Everitt, Brian (1980). *Cluster Analysis*. London: Heinemann Educational Books.

Everitt, Brian and Hothorn Torsten (2010). *A Handbook of Statistical Analysis Using R*. Boca Raton, FL: CRC Press.

Fairley, Jerry P. (2016). *Models and Modeling: An Introduction for Earth and Environmental Scientists*. John Wiley and Sons.

Fairley, Jerry P. and Jennifer J. Hinds (2004). "Rapid Transport Pathways for Geothermal Fluids in an Active Great Basin Fault Zone". In: *Geology* 32, pp. 825–828.

Fairley, Jerry P and Kirsten N Nicholson (2006). "Imaging lateral groundwater flow in the shallow subsurface using stochastic temperature fields". In: *Journal of Hydrology* 321.1, pp. 276–285.

Fairley, Jerry, James Heffner, and Jennifer Hinds (2003). "Geostatistical Evaluation of Permeability in an Active Fault Zone". In: *Geophysical Research Letters* 30, pp. 5-1–5-4.

Faulds, James E. et al. (2006). "Characterizing Structural Controls of Geothermal Fields in Northwestern Great Basin: A Progress Report". In: *GRC Transactions* 30, pp. 69–76.

Fournier, R.O., D.D. White, and A.H. Truesdell (1976). "Convective heat flow in Yellowstone National Park". In: *Proceedings of the United Nations Symposium on the Development and Uses of Geothermal Resources* 1, pp. 731–739.

Fournier, Robert O. (1989). "Geochemistry and Dynamics of the Yellowstone National Park Hydrothermal System". In: *Annual Review of Earth and Planetary Sciences* 17, pp. 13–52.

Güler, Cüneyt, Geoffrey D. Thyne, and John E. McCray (2002). "Evaluation of Graphical and Multivariate Statistical Methods for Classification of Water Chemistry Data". In: *Hydrogeology Journal* 10, pp. 455–474.

Heffner, James and Jerry Fairley (2006). "Using surface characteristics to infer the permeability structure of an active fault zone". In: *Sedimentary Geology* 184.3. Heterogeneity in Sedimentary Aquifers: Challenges for Characterization and Flow Modeling, pp. 255–265. ISSN: 0037-0738. DOI: https://doi.org/10.1016/j.sedgeo.2005.11.019. URL: http://www.sciencedirect.com/science/article/pii/S0037073805003751.

Hochstein, Manfred P. and Christopher J. Bromley (2005). "Measurement of heat flux from steaming ground". In: *Geothermics* 34.2, pp. 131–158. ISSN: 0375-6505. DOI: https://doi.org/10.1016/j.geothermics.2004.04.002.

Incropera, Frank P. et al. (2007). *Fundamentals of Heat and Mass Transfer*. Sixth. John Wiley and Sons.

Irawan, D.E. et al. (2009). "Hydrogeochemistry of volcanic hydrogeology based on cluster analysis of Mount Ciremai, West Java, Indonesia". In: *Journal of Hydrology* 376, pp. 221–234.

Jiang, Daxin, Chun Tang, and Aidong Zhang (2004). "Cluster Analysis for Gene Expression Data: A Survey". In: *IEEE Transactions on Knowledge and Data Engineering* 16.11, pp. 1370–1386.

Lindsey, Cary R. et al. (2018). "Cluster analysis as a tool for evaluating the exploration potential of Known Geothermal Resource Areas". In: *Geothermics* 72, pp. 358–370. ISSN: 0375-6505. DOI: `https://doi.org/10.1016/j.geothermics.2017.12.009`. URL: `http://www.sciencedirect.com/science/article/pii/S0375650517302626`.

Lubenow, Brady L. et al. (2016). "Influences on shallow ground temperatures in high flux thermal systems". In: *Journal of Volcanology and Geothermal Research* 323, pp. 53–61.

Marler, George D. (1964). *Studies of Geysers and Hot Springs along the Firehole River*. Yellowstone National Park: Yellowstone Library and Museum Association.

Mayer, J.M. et al. (2014). "Application of statistical approaches to analyze geological, geotechnical and hydrogeological data at a fractured-rock mine site in Northern Canada". In: *Hydrogeology Journal* 22.7, pp. 1707–1723.

McMillan, N.J. et al. (2016). "A heavy water doping method for measuring mass and thermal discharge from Yellowstone hot springs". In: *In Review*.

McMillan, N. et al. (2018). "heavy water doping method for measuring mass and thermal discharge from Yellowstone hot springs, in review". In: *Geosphere*.

Micklethwaite, Steven and Stephen F Cox (2004). "Fault-segment rupture, aftershock-zone fluid flow, and mineralization". In: *Geology* 32.9, pp. 813–816.

Mohamad, Ismail Bin and Dauda Usman (2013). "Standardization and its effects on k-means clustering algorithm". In: *Research Journal of Applied Sciences, Engineering, and Technology* 6.17, pp. 3299–3303.

Morgan, Paul et al. (1977). "Heat flow measurements in Yellowstone Lake and the thermal structure of the Yellowstone Caldera". In: *Journal of Geophysical Research* 82.26, pp. 3719–

3732. ISSN: 2156-2202. DOI: 10.1029/JB082i026p03719. URL: http://dx.doi.org/10.1029/JB082i026p03719.

Muffler, L.J.P., D.E. White, and A.H. Truesdell (1971). "Hydrothermal explosion craters in Yellowstone National Park". In: *Bulletin of Geological Society of America* 82, pp. 723–740.

Muffler, L.J. et al. (1982). *Geologic map of Lower Geyser Basin, Yellowstone National Park, Wyoming*.

Nelson, Carl E. and David L. Giles (1985). "Hydrothermal Eruption Mechanisms and Hot Spring Deposits". In: *Economic Geology* 80, pp. 1633–1639.

Nicholson, Keith (1993). *Geothermal Fluids: Chemistry and Exploration Techniques*. Berlin: Springer–Verlag.

Pickering, G., J.M. Bull, and D.J. Sanderson (1995). "Sampling power-law distributions". In: *Tectonophysics* 248.1, pp. 1–20. ISSN: 0040-1951.

Price, Adam N., Cary R. Lindsey, and Jerry P. Fairley (2017). "Interpretation of Ground Temperature Anomalies in Hydrothermal Discharge Areas". In: *Water Resources Research* 53.12, pp. 10173–10187. ISSN: 1944-7973. DOI: 10.1002/2017WR021077. URL: http://dx.doi.org/10.1002/2017WR021077.

Punj, Girish and David W. Stewart (1983). "Cluster Analysis in Marketing Research: Review and Suggestions for Application". In: *Journal of Marketing Research* 20, pp. 134–148.

R Core Team (2014). *R: A Language and Environment for Statistical Computing*. R Foundation for Statistical Computing. Vienna, Austria. URL: http://www.R-project.org/.

Rodman, A. and C. Guiles (2008). "Greater Yellowstone Science Learning Center and the Yellowstone thermal inventory". In: *Geothermal Biology and Geochemistry in Yellowstone National Park*. Ed. by W. Inskeep and J. Peters. NSF Research Coordination Network and Montana State University Thermal Biology Institute Workshop, January 10–13.

Rowland, J.C., M. Manga, and T.P. Rose (2008). "The Influence of Poorly Interconnected Fault Zone Flow Paths on Spring Geochemistry". In: *Geofluids* 8, pp. 93–101.

Seward, Anya et al. (2018). "Improved environmental monitoring of surface geothermal features through comparisons of thermal infrared, satellite remote sensing and terrestrial calorimetry". In: *Geothermics* 73, pp. 60–73. ISSN: 0375-6505. DOI: https://doi.org/10.1016/j.

geothermics.2018.01.007. URL: `http://www.sciencedirect.com/science/article/pii/S0375650517302651`.

Snoeyink, Vernon L. and David Jenkins (1980). *Water Chemistry*. New York, N.Y.: John Wiley and Sons.

Sorey, Michael L. and M. Colvard Elizabeth (1994). *Measurements of heat and mass flow from thermal areas in Lassen Volcanic National Park, California, 1984-93*. Water Resources Investigations Report 94-4180-A. U.S. Geological Survey.

Souto, Marcilio C.P. de et al. (2008). "Comparative Study on Normalization Procedures for Cluster Analysis of Gene Expression Datasets". In: *Proceedings of the Internation Joint Conference on Neural Networks*, pp. 2792–2798.

Tan, Pang-Ning, Michael Steinbach, and Vipin Kumar (2006). *Introduction to Data Mining*. Boston, MA: Pearson Addison.

Terada, Akihiko, Tsuneomi Kagiyama, and Hiromitsu Oshima (2008). "Ice Box Calorimetry: A useful method for estimating heat discharge rates through steaming ground". In: *Earth, Planets and Space* 60.6, pp. 699–703. ISSN: 1880-5981. DOI: 10.1186/BF03353133. URL: `https://doi.org/10.1186/BF03353133`.

Tester, Jefferson W. et al. (2006). *The Future of Geothermal Energy: Impact of Enhanced Geothermal Systems (EGS) on the United States in the 21st Century*.

Truesdell, Alfred H., Manuel Nathenson, and Robert O. Rye. "The effects of subsurface boiling and dilution on the isotopic compositions of Yellowstone thermal waters". In: *Journal of Geophysical Research* 82.26, pp. 3694–3704. DOI: 10.1029/JB082i026p03694.

VanTrump, George and A.T. Miesch (1977). "The US Geological Survey RASS-STATPAC System for Management and Statistical Reduction of Geochemical Data". In: *Computers and Geosciences* 3, pp. 475–488.

Vaughan, R. Greg et al. (2012). "Mapping temperature and radiant geothermal heat flux anomalies in the Yellowstone geothermal system using ASTER thermal infrared data". In: *GRC Transactions* 36, pp. 1403–1410.

Veldeman, E. et al. (1990). "Thermal Waters from South Bulgaria: A multivariate approach for evaluation and interpretation of analytical data". In: *Geothermal Resources Council Transactions* 14, pp. 1537–1543.

White, Donald E. (1969). "Rapid heat-flow surveying of geothermal areas, utilizing individual snowfalls as calorimeters". In: *Journal of Geophysical Research* 74.22, pp. 5191–5201. ISSN: 2156-2202. DOI: 10.1029/JB074i022p05191. URL: http://dx.doi.org/10.1029/JB074i022p05191.

Wood, Scott A. (2005). "Rare earth element systematics of acidic geothermal waters from Taupo Volcanic Zone, New Zealand". In: *Journal of Geochemical Exploration* 89.1, pp. 424–427.

Yuhara, Kozo (1970). "Heat transfer measurement in a geothermal area". In: *Tectonphysics* 10, pp. 19–30.

Appendix A

R Script for geostatistical analysis of heat flux and temperature

A.1 Bravo Temperatures

Load spatial analysis package

>library(geoR)

Read in data file "Bravo.txt"

Convert to geodata

>BT=as.geodata(Bravo)

Create variogram

>BTvgm=variog(BT, max.dist=50) >plot(BTvgm,pch=19)

Manually fitting line by eye

(nugget = 0.25, sill = 14, range = 27)

>lines.variomodel(cov.model="sph", cov.pars=c(14,27), kappa = 1,nug=0.25,max.dist=50, lwd=2)

>text(x=30, y=2, labels=("nugget = 0.25, sill = 14, range = 27"))

Creating the grid to plot contours

>loci=expand.grid(seq(0,72,by=0.50),seq(0,72, by=0.50))

>str(loci)

>plot(loci)

>kcT=krige.conv(BT, loc=loci, krige=krige.control(cov.model="sph" ,cov.pars=c(14,27),nugget=0.25))

Plotting contour maps

gray

>contour(kcT,filled=TRUE, nlevels=10,col=rev(gray.colors(12, start=0.2, end=0.7)), lwd=1)

heat colors

>contour(kcT,filled=TRUE, nlevels=10,col=rev(heat.colors(12)), lwd=1)

A.2   Bravo Heat Flux

Load spatial analysis package

>library(geoR)

Read in data file "fluxdata.txt"

Convert to geodata

>BT=as.geodata(fluxdata)

Create variogram

>BTFvgm=variog(BF, max.dist=50) >plot(BFvgm,pch=19)

Manually fitting line by eye

(nugget = 2.5, sill = 13, range = 12)

>lines.variomodel(cov.model="sph", cov.pars=c(13,12), nug=2.5,max.dist=30, lwd=2, pch=19)

>text(x=8, y=2, labels="nugget = 2.5, sill = 13, range = 12")

Creating the grid to plot contours

>loci=expand.grid(seq(0,72,by=0.50),seq(0,72, by=0.50))

>str(loci)

>plot(loci)

>kcF=krige.conv(BF, loc=loci, krige=krige.control(cov.model="sph" ,cov.pars=c(13,12),nugget=2.5))

Plotting contour maps

gray

>contour(kcF,filled=TRUE, nlevels=10,col=rev(gray.colors(12, start=0.2, end=0.7)), lwd=1)

heat colors

>contour(kcT,filled=TRUE, nlevels=10,col=rev(heat.colors(12)), lwd=1)

Calculate total watts

sum of flux values

>summary(kcF$predict)

times area of grid square

>sum(kcF$predict)*0.25

Appendix B

Nusselt heat flux calculation data table

x	y	T_{20}	T_f	T_∞	k	ρ	μ	C_p	ν	α	β	Pr	L	Gr	Ra	Nu_L	h	q_{adv}	q_{cond}
0	3	22.3	21.8	21.28	2.6E-02	1.2E+00	1.9E-05	1.0E+03	1.5E-05	2.1E-05	3.4E-03	0.72	6.75	2.2E+10	1.6E+10	292.24	1.11	0.57	0.57
0	6	23.7	22.5	21.28	2.6E-02	1.2E+00	1.9E-05	1.0E+03	1.5E-05	2.1E-05	3.4E-03	0.72	6.75	5.2E+10	3.7E+10	384.74	1.46	1.77	1.77
0	9	23.1	22.2	21.28	2.6E-02	1.2E+00	1.9E-05	1.0E+03	1.5E-05	2.1E-05	3.4E-03	0.72	6.75	3.9E+10	2.8E+10	351.31	1.34	1.22	1.22
0	18	22.0	21.5	20.95	2.6E-02	1.2E+00	1.8E-05	1.0E+03	1.5E-05	2.1E-05	3.4E-03	0.72	6.75	2.3E+10	1.6E+10	295.28	1.12	0.59	0.59
0	21	22.1	21.5	20.95	2.6E-02	1.2E+00	1.8E-05	1.0E+03	1.5E-05	2.1E-05	3.4E-03	0.72	6.75	2.5E+10	1.8E+10	303.93	1.16	0.67	0.67
0	24	21.8	21.4	20.95	2.6E-02	1.2E+00	1.8E-05	1.0E+03	1.5E-05	2.1E-05	3.4E-03	0.72	6.75	1.8E+10	1.3E+10	276.15	1.05	0.45	0.45
3	21	21.8	21.4	20.95	2.6E-02	1.2E+00	1.8E-05	1.0E+03	1.5E-05	2.1E-05	3.4E-03	0.72	6.75	1.8E+10	1.3E+10	276.15	1.05	0.45	0.45
3	24	22.6	21.8	20.95	2.6E-02	1.2E+00	1.8E-05	1.0E+03	1.5E-05	2.1E-05	3.4E-03	0.72	6.75	3.6E+10	2.6E+10	340.91	1.30	1.07	1.07
3	27	21.0	21.0	20.95	2.6E-02	1.2E+00	1.8E-05	1.0E+03	1.5E-05	2.1E-05	3.4E-03	0.72	6.75	1.1E+09	7.8E+08	113.93	0.43	0.01	0.01
6	6	21.3	21.3	21.28	2.6E-02	1.2E+00	1.9E-05	1.0E+03	1.5E-05	2.1E-05	3.4E-03	0.72	6.75	4.3E+08	3.1E+08	86.00	0.33	0.00	0.00
6	15	21.4	21.2	20.95	2.6E-02	1.2E+00	1.8E-05	1.0E+03	1.5E-05	2.1E-05	3.4E-03	0.72	6.75	9.7E+09	7.0E+09	225.88	0.86	0.19	0.19
6	18	21.6	21.3	20.95	2.6E-02	1.2E+00	1.8E-05	1.0E+03	1.5E-05	2.1E-05	3.4E-03	0.72	6.75	1.4E+10	1.0E+10	253.67	0.97	0.31	0.31
6	21	21.6	21.3	20.95	2.6E-02	1.2E+00	1.8E-05	1.0E+03	1.5E-05	2.1E-05	3.4E-03	0.72	6.75	1.4E+10	1.0E+10	253.67	0.97	0.31	0.31
6	24	22.2	21.6	20.95	2.6E-02	1.2E+00	1.8E-05	1.0E+03	1.5E-05	2.1E-05	3.4E-03	0.72	6.75	2.7E+10	1.9E+10	312.09	1.19	0.74	0.74
6	36	21.4	20.5	19.60	2.6E-02	1.2E+00	1.8E-05	1.0E+03	1.5E-05	2.1E-05	3.4E-03	0.72	6.75	4.0E+10	2.8E+10	352.17	1.34	1.21	1.21
9	27	21.0	21.0	20.95	2.6E-02	1.2E+00	1.8E-05	1.0E+03	1.5E-05	2.1E-05	3.4E-03	0.72	6.75	1.1E+09	7.8E+08	113.93	0.43	0.01	0.01
9	30	21.6	21.3	20.95	2.6E-02	1.2E+00	1.8E-05	1.0E+03	1.5E-05	2.1E-05	3.4E-03	0.72	6.75	1.4E+10	1.0E+10	253.67	0.97	0.31	0.31
9	33	22.6	21.8	20.95	2.6E-02	1.2E+00	1.8E-05	1.0E+03	1.5E-05	2.1E-05	3.4E-03	0.72	6.75	3.6E+10	2.6E+10	340.91	1.30	1.07	1.07
9	36	21.6	20.6	19.60	2.6E-02	1.2E+00	1.8E-05	1.0E+03	1.5E-05	2.1E-05	3.4E-03	0.72	6.75	4.4E+10	3.2E+10	364.20	1.39	1.39	1.39
9	39	20.2	19.9	19.60	2.6E-02	1.2E+00	1.8E-05	1.0E+03	1.5E-05	2.1E-05	3.4E-03	0.72	6.75	1.3E+10	9.5E+09	248.52	0.95	0.28	0.28
12	27	21.7	21.3	20.95	2.6E-02	1.2E+00	1.8E-05	1.0E+03	1.5E-05	2.1E-05	3.4E-03	0.72	6.75	1.6E+10	1.2E+10	265.42	1.01	0.38	0.38
12	30	22.3	21.6	20.95	2.6E-02	1.2E+00	1.8E-05	1.0E+03	1.5E-05	2.1E-05	3.4E-03	0.72	6.75	2.9E+10	2.1E+10	319.82	1.22	0.82	0.82
12	33	22.9	21.9	20.95	2.6E-02	1.2E+00	1.8E-05	1.0E+03	1.5E-05	2.1E-05	3.4E-03	0.72	6.75	4.2E+10	3.0E+10	359.54	1.37	1.33	1.33
12	36	22.4	21.0	19.60	2.6E-02	1.2E+00	1.8E-05	1.0E+03	1.5E-05	2.1E-05	3.4E-03	0.72	6.75	6.2E+10	4.4E+10	405.51	1.54	2.16	2.16
12	39	22.2	20.9	19.60	2.6E-02	1.2E+00	1.8E-05	1.0E+03	1.5E-05	2.1E-05	3.4E-03	0.72	6.75	5.7E+10	4.1E+10	396.02	1.51	1.96	1.96
12	42	20.8	20.2	19.60	2.6E-02	1.2E+00	1.8E-05	1.0E+03	1.5E-05	2.1E-05	3.4E-03	0.72	6.75	2.6E+10	1.9E+10	309.55	1.18	0.71	0.71
12	45	19.7	19.7	19.60	2.6E-02	1.2E+00	1.8E-05	1.0E+03	1.5E-05	2.1E-05	3.4E-03	0.72	6.75	2.2E+09	1.6E+09	141.79	0.54	0.03	0.03
15	3	22.2	21.7	21.28	2.6E-02	1.2E+00	1.9E-05	1.0E+03	1.5E-05	2.1E-05	3.4E-03	0.72	6.75	2.0E+10	1.4E+10	282.83	1.08	0.50	0.50
15	27	23.4	22.2	20.95	2.6E-02	1.2E+00	1.8E-05	1.0E+03	1.5E-05	2.1E-05	3.4E-03	0.72	6.75	5.3E+10	3.8E+10	386.71	1.47	1.80	1.80

x	y	T_{20}	T_f	T_∞	k	ρ	μ	C_p	ν	α	β	Pr	L	Gr	Ra	Nu_L	h	q_{adv}	q_{cond}
15	30	24.6	22.8	20.95	2.6E-02	1.2E+00	1.8E-05	1.0E+03	1.5E-05	2.1E-05	3.4E-03	0.72	6.75	7.9E+10	5.7E+10	439.29	1.67	3.05	3.05
15	33	24.9	22.9	20.95	2.6E-02	1.2E+00	1.8E-05	1.0E+03	1.5E-05	2.1E-05	3.4E-03	0.72	6.75	8.5E+10	6.1E+10	450.54	1.72	3.39	3.39
15	36	23.2	21.4	19.60	2.6E-02	1.2E+00	1.8E-05	1.0E+03	1.5E-05	2.1E-05	3.4E-03	0.72	6.75	7.9E+10	5.7E+10	439.46	1.67	3.01	3.01
15	39	23.9	21.8	19.60	2.6E-02	1.2E+00	1.8E-05	1.0E+03	1.5E-05	2.1E-05	3.4E-03	0.72	6.75	9.5E+10	6.8E+10	465.21	1.77	3.81	3.81
15	42	25.0	22.3	19.60	2.6E-02	1.2E+00	1.8E-05	1.0E+03	1.5E-05	2.1E-05	3.4E-03	0.72	6.75	1.2E+11	8.5E+10	500.48	1.91	5.14	5.14
15	45	22.5	21.1	19.60	2.6E-02	1.2E+00	1.8E-05	1.0E+03	1.5E-05	2.1E-05	3.4E-03	0.72	6.75	6.4E+10	4.6E+10	410.09	1.56	2.26	2.26
18	21	24.4	22.7	20.95	2.6E-02	1.2E+00	1.8E-05	1.0E+03	1.5E-05	2.1E-05	3.4E-03	0.72	6.75	7.5E+10	5.4E+10	431.43	1.64	2.83	2.83
18	27	23.0	22.0	20.95	2.6E-02	1.2E+00	1.8E-05	1.0E+03	1.5E-05	2.1E-05	3.4E-03	0.72	6.75	4.4E+10	3.2E+10	365.32	1.39	1.43	1.43
18	30	23.8	22.4	20.95	2.6E-02	1.2E+00	1.8E-05	1.0E+03	1.5E-05	2.1E-05	3.4E-03	0.72	6.75	6.2E+10	4.4E+10	405.85	1.55	2.20	2.20
18	33	24.2	22.6	20.95	2.6E-02	1.2E+00	1.8E-05	1.0E+03	1.5E-05	2.1E-05	3.4E-03	0.72	6.75	7.0E+10	5.1E+10	423.27	1.61	2.62	2.62
18	36	24.0	21.8	19.60	2.6E-02	1.2E+00	1.8E-05	1.0E+03	1.5E-05	2.1E-05	3.4E-03	0.72	6.75	9.7E+10	7.0E+10	468.65	1.78	3.93	3.93
18	39	26.0	22.8	19.60	2.6E-02	1.2E+00	1.8E-05	1.0E+03	1.5E-05	2.1E-05	3.4E-03	0.72	6.75	1.4E+11	1.0E+11	528.55	2.01	6.44	6.44
18	42	24.9	22.3	19.60	2.6E-02	1.2E+00	1.8E-05	1.0E+03	1.5E-05	2.1E-05	3.4E-03	0.72	6.75	1.2E+11	8.4E+10	497.48	1.89	5.02	5.02
18	45	23.3	21.5	19.60	2.6E-02	1.2E+00	1.8E-05	1.0E+03	1.5E-05	2.1E-05	3.4E-03	0.72	6.75	8.1E+10	5.9E+10	443.34	1.69	3.12	3.12
21	24	21.2	21.1	20.95	2.6E-02	1.2E+00	1.8E-05	1.0E+03	1.5E-05	2.1E-05	3.4E-03	0.72	6.75	5.4E+09	3.9E+09	187.79	0.72	0.09	0.09
21	27	22.9	21.9	20.95	2.6E-02	1.2E+00	1.8E-05	1.0E+03	1.5E-05	2.1E-05	3.4E-03	0.72	6.75	4.2E+10	3.0E+10	359.54	1.37	1.33	1.33
21	30	22.5	21.7	20.95	2.6E-02	1.2E+00	1.8E-05	1.0E+03	1.5E-05	2.1E-05	3.4E-03	0.72	6.75	3.3E+10	2.4E+10	334.19	1.27	0.99	0.99
21	33	26.7	23.8	20.95	2.6E-02	1.2E+00	1.8E-05	1.0E+03	1.5E-05	2.1E-05	3.4E-03	0.72	6.75	1.2E+11	8.9E+10	508.21	1.93	5.56	5.56
21	42	27.1	23.4	19.60	2.6E-02	1.2E+00	1.8E-05	1.0E+03	1.5E-05	2.1E-05	3.4E-03	0.72	6.75	1.7E+11	1.2E+11	556.20	2.12	7.94	7.94
21	45	22.3	21.0	19.60	2.6E-02	1.2E+00	1.8E-05	1.0E+03	1.5E-05	2.1E-05	3.4E-03	0.72	6.75	5.9E+10	4.3E+10	400.82	1.53	2.06	2.06
21	48	24.4	22.5	20.61	2.6E-02	1.2E+00	1.8E-05	1.0E+03	1.5E-05	2.1E-05	3.4E-03	0.72	6.75	8.2E+10	5.9E+10	445.15	1.69	3.21	3.21
24	21	22.5	21.7	20.95	2.6E-02	1.2E+00	1.8E-05	1.0E+03	1.5E-05	2.1E-05	3.4E-03	0.72	6.75	3.3E+10	2.4E+10	334.19	1.27	0.99	0.99
24	27	22.5	21.7	20.95	2.6E-02	1.2E+00	1.8E-05	1.0E+03	1.5E-05	2.1E-05	3.4E-03	0.72	6.75	3.3E+10	2.4E+10	334.19	1.27	0.99	0.99
24	30	22.8	21.9	20.95	2.6E-02	1.2E+00	1.8E-05	1.0E+03	1.5E-05	2.1E-05	3.4E-03	0.72	6.75	4.0E+10	2.9E+10	353.56	1.35	1.25	1.25
24	42	28.2	23.9	19.60	2.6E-02	1.2E+00	1.8E-05	1.0E+03	1.5E-05	2.1E-05	3.4E-03	0.72	6.75	1.9E+11	1.4E+11	581.24	2.21	9.52	9.52
24	45	26.3	23.0	19.60	2.6E-02	1.2E+00	1.8E-05	1.0E+03	1.5E-05	2.1E-05	3.4E-03	0.72	6.75	1.5E+11	1.1E+11	536.39	2.04	6.84	6.84
24	48	23.3	22.0	20.61	2.6E-02	1.2E+00	1.8E-05	1.0E+03	1.5E-05	2.1E-05	3.4E-03	0.72	6.75	5.8E+10	4.2E+10	398.91	1.52	2.04	2.04
27	27	22.3	21.6	20.95	2.6E-02	1.2E+00	1.8E-05	1.0E+03	1.5E-05	2.1E-05	3.4E-03	0.72	6.75	2.9E+10	2.1E+10	319.82	1.22	0.82	0.82
27	30	22.8	21.9	20.95	2.6E-02	1.2E+00	1.8E-05	1.0E+03	1.5E-05	2.1E-05	3.4E-03	0.72	6.75	4.0E+10	2.9E+10	353.56	1.35	1.25	1.25
27	45	32.9	26.3	19.60	2.6E-02	1.2E+00	1.8E-05	1.0E+03	1.5E-05	2.1E-05	3.4E-03	0.72	6.75	2.9E+11	2.1E+11	668.94	2.55	16.94	16.94
27	48	24.0	22.3	20.61	2.6E-02	1.2E+00	1.8E-05	1.0E+03	1.5E-05	2.1E-05	3.4E-03	0.72	6.75	7.4E+10	5.3E+10	429.54	1.64	2.77	2.77

x	y	T_{20}	T_f	T_∞	k	ρ	μ	C_p	ν	α	β	Pr	L	Gr	Ra	Nu_L	h	q_{adv}	q_{cond}
30	27	26.1	23.5	20.95	2.6E-02	1.2E+00	1.8E-05	1.0E+03	1.5E-05	2.1E-05	3.4E-03	0.72	6.75	1.1E+11	8.0E+10	490.54	1.87	4.81	4.81
30	30	23.3	22.1	20.95	2.6E-02	1.2E+00	1.8E-05	1.0E+03	1.5E-05	2.1E-05	3.4E-03	0.72	6.75	5.1E+10	3.7E+10	381.60	1.45	1.71	1.71
30	42	28.3	24.0	19.60	2.6E-02	1.2E+00	1.8E-05	1.0E+03	1.5E-05	2.1E-05	3.4E-03	0.72	6.75	1.9E+11	1.4E+11	583.41	2.22	9.66	9.66
30	45	27.1	23.4	19.60	2.6E-02	1.2E+00	1.8E-05	1.0E+03	1.5E-05	2.1E-05	3.4E-03	0.72	6.75	1.7E+11	1.2E+11	556.20	2.12	7.94	7.94
30	48	23.9	22.3	20.61	2.6E-02	1.2E+00	1.8E-05	1.0E+03	1.5E-05	2.1E-05	3.4E-03	0.72	6.75	7.1E+10	5.1E+10	425.44	1.62	2.66	2.66
33	33	29.8	25.4	20.95	2.6E-02	1.2E+00	1.8E-05	1.0E+03	1.5E-05	2.1E-05	3.4E-03	0.72	6.75	1.9E+11	1.4E+11	583.80	2.22	9.84	9.84
33	39	29.3	24.5	19.60	2.6E-02	1.2E+00	1.8E-05	1.0E+03	1.5E-05	2.1E-05	3.4E-03	0.72	6.75	2.1E+11	1.5E+11	604.22	2.30	11.16	11.16
33	42	22.0	20.8	19.60	2.6E-02	1.2E+00	1.8E-05	1.0E+03	1.5E-05	2.1E-05	3.4E-03	0.72	6.75	5.3E+10	3.8E+10	386.02	1.47	1.76	1.76
36	27	22.0	21.5	20.95	2.6E-02	1.2E+00	1.8E-05	1.0E+03	1.5E-05	2.1E-05	3.4E-03	0.72	6.75	2.3E+10	1.6E+10	295.28	1.12	0.59	0.59
36	30	23.8	22.4	20.95	2.6E-02	1.2E+00	1.8E-05	1.0E+03	1.5E-05	2.1E-05	3.4E-03	0.72	6.75	6.2E+10	4.4E+10	405.85	1.55	2.20	2.20
36	33	25.6	23.3	20.95	2.6E-02	1.2E+00	1.8E-05	1.0E+03	1.5E-05	2.1E-05	3.4E-03	0.72	6.75	1.0E+11	7.2E+10	474.73	1.81	4.20	4.20
36	39	23.1	21.4	19.60	2.6E-02	1.2E+00	1.8E-05	1.0E+03	1.5E-05	2.1E-05	3.4E-03	0.72	6.75	7.7E+10	5.5E+10	435.52	1.66	2.90	2.90
36	42	24.9	22.3	19.60	2.6E-02	1.2E+00	1.8E-05	1.0E+03	1.5E-05	2.1E-05	3.4E-03	0.72	6.75	1.2E+11	8.4E+10	497.48	1.89	5.02	5.02
42	0	21.9	20.9	19.93	2.6E-02	1.2E+00	1.8E-05	1.0E+03	1.5E-05	2.1E-05	3.4E-03	0.72	6.75	4.3E+10	3.1E+10	362.03	1.38	1.36	1.36
45	0	21.5	20.7	19.93	2.6E-02	1.2E+00	1.8E-05	1.0E+03	1.5E-05	2.1E-05	3.4E-03	0.72	6.75	3.4E+10	2.5E+10	336.77	1.28	1.01	1.01
45	3	22.0	21.0	19.93	2.6E-02	1.2E+00	1.8E-05	1.0E+03	1.5E-05	2.1E-05	3.4E-03	0.72	6.75	4.5E+10	3.3E+10	367.79	1.40	1.45	1.45
45	6	21.6	20.8	19.93	2.6E-02	1.2E+00	1.8E-05	1.0E+03	1.5E-05	2.1E-05	3.4E-03	0.72	6.75	3.7E+10	2.6E+10	343.46	1.31	1.09	1.09
45	9	22.3	21.1	19.93	2.6E-02	1.2E+00	1.8E-05	1.0E+03	1.5E-05	2.1E-05	3.4E-03	0.72	6.75	5.2E+10	3.7E+10	384.02	1.46	1.73	1.73
45	18	21.3	20.8	20.27	2.6E-02	1.2E+00	1.8E-05	1.0E+03	1.5E-05	2.1E-05	3.4E-03	0.72	6.75	2.2E+10	1.6E+10	294.19	1.12	0.58	0.58
45	21	20.7	20.5	20.27	2.6E-02	1.2E+00	1.8E-05	1.0E+03	1.5E-05	2.1E-05	3.4E-03	0.72	6.75	9.4E+09	6.7E+09	223.20	0.85	0.18	0.18
45	24	20.8	20.5	20.27	2.6E-02	1.2E+00	1.8E-05	1.0E+03	1.5E-05	2.1E-05	3.4E-03	0.72	6.75	1.2E+10	8.3E+09	238.41	0.91	0.24	0.24
45	30	20.3	20.3	20.27	2.6E-02	1.2E+00	1.8E-05	1.0E+03	1.5E-05	2.1E-05	3.4E-03	0.72	6.75	6.5E+08	4.7E+08	97.64	0.37	0.01	0.01
48	0	23.1	21.5	19.93	2.6E-02	1.2E+00	1.8E-05	1.0E+03	1.5E-05	2.1E-05	3.4E-03	0.72	6.75	6.9E+10	5.0E+10	421.43	1.60	2.54	2.54
48	3	23.0	21.5	19.93	2.6E-02	1.2E+00	1.8E-05	1.0E+03	1.5E-05	2.1E-05	3.4E-03	0.72	6.75	6.7E+10	4.8E+10	417.13	1.59	2.44	2.44
48	6	26.5	23.2	19.93	2.6E-02	1.2E+00	1.8E-05	1.0E+03	1.5E-05	2.1E-05	3.4E-03	0.72	6.75	1.4E+11	1.0E+11	532.39	2.03	6.66	6.66
48	9	28.5	24.2	19.93	2.6E-02	1.2E+00	1.8E-05	1.0E+03	1.5E-05	2.1E-05	3.4E-03	0.72	6.75	1.9E+11	1.3E+11	579.90	2.21	9.46	9.46
48	12	25.6	22.8	19.93	2.6E-02	1.2E+00	1.8E-05	1.0E+03	1.5E-05	2.1E-05	3.4E-03	0.72	6.75	1.2E+11	8.9E+10	507.78	1.93	5.48	5.48
48	15	20.7	20.5	20.27	2.6E-02	1.2E+00	1.8E-05	1.0E+03	1.5E-05	2.1E-05	3.4E-03	0.72	6.75	9.4E+09	6.7E+09	223.20	0.85	0.18	0.18
48	18	20.4	20.3	20.27	2.6E-02	1.2E+00	1.8E-05	1.0E+03	1.5E-05	2.1E-05	3.4E-03	0.72	6.75	2.8E+09	2.0E+09	153.48	0.58	0.04	0.04
48	21	28.1	24.2	20.27	2.6E-02	1.2E+00	1.8E-05	1.0E+03	1.5E-05	2.1E-05	3.4E-03	0.72	6.75	1.7E+11	1.2E+11	562.60	2.14	8.39	8.39
48	24	25.5	22.9	20.27	2.6E-02	1.2E+00	1.8E-05	1.0E+03	1.5E-05	2.1E-05	3.4E-03	0.72	6.75	1.1E+11	8.2E+10	494.18	1.88	4.92	4.92

x	y	T_{20}	T_f	T_∞	k	ρ	μ	C_p	ν	α	β	Pr	L	Gr	Ra	Nu_L	h	q_{adv}	q_{cond}
48	27	21.5	20.9	20.27	2.6E-02	1.2E+00	1.8E-05	1.0E+03	1.5E-05	2.1E-05	3.4E-03	0.72	6.75	2.7E+10	1.9E+10	311.24	1.19	0.73	0.73
48	30	21.2	20.7	20.27	2.6E-02	1.2E+00	1.8E-05	1.0E+03	1.5E-05	2.1E-05	3.4E-03	0.72	6.75	2.0E+10	1.5E+10	284.81	1.08	0.50	0.50
48	33	22.9	21.6	20.27	2.6E-02	1.2E+00	1.8E-05	1.0E+03	1.5E-05	2.1E-05	3.4E-03	0.72	6.75	5.7E+10	4.1E+10	396.53	1.51	1.99	1.99
48	36	20.6	20.4	20.27	2.6E-02	1.2E+00	1.8E-05	1.0E+03	1.5E-05	2.1E-05	3.4E-03	0.72	6.75	7.2E+09	5.2E+09	205.37	0.78	0.13	0.13
51	0	26.6	23.3	19.93	2.6E-02	1.2E+00	1.8E-05	1.0E+03	1.5E-05	2.1E-05	3.4E-03	0.72	6.75	1.5E+11	1.1E+11	534.98	2.04	6.79	6.79
51	3	24.1	22.0	19.93	2.6E-02	1.2E+00	1.8E-05	1.0E+03	1.5E-05	2.1E-05	3.4E-03	0.72	6.75	9.1E+10	6.6E+10	460.11	1.75	3.65	3.65
51	6	23.3	21.6	19.93	2.6E-02	1.2E+00	1.8E-05	1.0E+03	1.5E-05	2.1E-05	3.4E-03	0.72	6.75	7.4E+10	5.3E+10	429.77	1.64	2.76	2.76
51	9	26.2	23.1	19.93	2.6E-02	1.2E+00	1.8E-05	1.0E+03	1.5E-05	2.1E-05	3.4E-03	0.72	6.75	1.4E+11	9.9E+10	524.45	2.00	6.26	6.26
51	12	25.5	22.7	19.93	2.6E-02	1.2E+00	1.8E-05	1.0E+03	1.5E-05	2.1E-05	3.4E-03	0.72	6.75	1.2E+11	8.8E+10	504.88	1.92	5.35	5.35
51	15	23.2	21.7	20.27	2.6E-02	1.2E+00	1.8E-05	1.0E+03	1.5E-05	2.1E-05	3.4E-03	0.72	6.75	6.4E+10	4.6E+10	410.46	1.56	2.29	2.29
51	18	26.3	23.3	20.27	2.6E-02	1.2E+00	1.8E-05	1.0E+03	1.5E-05	2.1E-05	3.4E-03	0.72	6.75	1.3E+11	9.5E+10	517.29	1.97	5.94	5.94
51	21	29.6	24.9	20.27	2.6E-02	1.2E+00	1.8E-05	1.0E+03	1.5E-05	2.1E-05	3.4E-03	0.72	6.75	2.0E+11	1.5E+11	595.26	2.27	10.57	10.57
51	24	27.2	23.7	20.27	2.6E-02	1.2E+00	1.8E-05	1.0E+03	1.5E-05	2.1E-05	3.4E-03	0.72	6.75	1.5E+11	1.1E+11	540.94	2.06	7.14	7.14
51	27	23.6	21.9	20.27	2.6E-02	1.2E+00	1.8E-05	1.0E+03	1.5E-05	2.1E-05	3.4E-03	0.72	6.75	7.3E+10	5.2E+10	427.61	1.63	2.71	2.71
51	30	21.5	20.9	20.27	2.6E-02	1.2E+00	1.8E-05	1.0E+03	1.5E-05	2.1E-05	3.4E-03	0.72	6.75	2.7E+10	1.9E+10	311.24	1.19	0.73	0.73
51	33	21.6	20.9	20.27	2.6E-02	1.2E+00	1.8E-05	1.0E+03	1.5E-05	2.1E-05	3.4E-03	0.72	6.75	2.9E+10	2.1E+10	319.07	1.21	0.81	0.81
51	36	24.3	22.3	20.27	2.6E-02	1.2E+00	1.8E-05	1.0E+03	1.5E-05	2.1E-05	3.4E-03	0.72	6.75	8.8E+10	6.3E+10	454.55	1.73	3.49	3.49
54	0	22.0	21.0	19.93	2.6E-02	1.2E+00	1.8E-05	1.0E+03	1.5E-05	2.1E-05	3.4E-03	0.72	6.75	4.5E+10	3.3E+10	367.79	1.40	1.45	1.45
54	3	25.7	22.8	19.93	2.6E-02	1.2E+00	1.8E-05	1.0E+03	1.5E-05	2.1E-05	3.4E-03	0.72	6.75	1.3E+11	9.1E+10	510.64	1.94	5.61	5.61
54	6	26.3	23.1	19.93	2.6E-02	1.2E+00	1.8E-05	1.0E+03	1.5E-05	2.1E-05	3.4E-03	0.72	6.75	1.4E+11	1.0E+11	527.13	2.01	6.39	6.39
54	9	27.3	23.6	19.93	2.6E-02	1.2E+00	1.8E-05	1.0E+03	1.5E-05	2.1E-05	3.4E-03	0.72	6.75	1.6E+11	1.2E+11	552.43	2.10	7.75	7.75
54	12	27.9	23.9	19.93	2.6E-02	1.2E+00	1.8E-05	1.0E+03	1.5E-05	2.1E-05	3.4E-03	0.72	6.75	1.7E+11	1.3E+11	566.51	2.16	8.60	8.60
54	15	27.6	23.9	20.27	2.6E-02	1.2E+00	1.8E-05	1.0E+03	1.5E-05	2.1E-05	3.4E-03	0.72	6.75	1.6E+11	1.1E+11	550.79	2.10	7.69	7.69
54	18	27.2	23.7	20.27	2.6E-02	1.2E+00	1.8E-05	1.0E+03	1.5E-05	2.1E-05	3.4E-03	0.72	6.75	1.5E+11	1.1E+11	540.94	2.06	7.14	7.14
54	21	30.1	25.2	20.27	2.6E-02	1.2E+00	1.8E-05	1.0E+03	1.5E-05	2.1E-05	3.4E-03	0.72	6.75	2.1E+11	1.5E+11	605.35	2.30	11.33	11.33
54	24	33.5	26.9	20.27	2.6E-02	1.2E+00	1.8E-05	1.0E+03	1.5E-05	2.1E-05	3.4E-03	0.72	6.75	2.9E+11	2.1E+11	666.20	2.54	16.78	16.78
54	27	29.5	24.9	20.27	2.6E-02	1.2E+00	1.8E-05	1.0E+03	1.5E-05	2.1E-05	3.4E-03	0.72	6.75	2.0E+11	1.4E+11	593.20	2.26	10.42	10.42
54	30	24.9	22.6	20.27	2.6E-02	1.2E+00	1.8E-05	1.0E+03	1.5E-05	2.1E-05	3.4E-03	0.72	6.75	1.0E+11	7.3E+10	475.23	1.81	4.19	4.19
54	33	23.4	21.8	20.27	2.6E-02	1.2E+00	1.8E-05	1.0E+03	1.5E-05	2.1E-05	3.4E-03	0.72	6.75	6.8E+10	4.9E+10	419.22	1.60	2.50	2.50
54	36	24.0	22.1	20.27	2.6E-02	1.2E+00	1.8E-05	1.0E+03	1.5E-05	2.1E-05	3.4E-03	0.72	6.75	8.1E+10	5.9E+10	443.42	1.69	3.15	3.15
54	39	25.2	23.2	21.28	2.6E-02	1.2E+00	1.9E-05	1.0E+03	1.5E-05	2.1E-05	3.4E-03	0.72	6.75	8.4E+10	6.1E+10	448.92	1.71	3.35	3.35

x	y	T_{20}	T_f	T_∞	k	ρ	μ	C_p	ν	α	β	Pr	L	Gr	Ra	Nu_L	h	q_{adv}	q_{cond}
54	45	21.9	21.6	21.28	2.6E-02	1.2E+00	1.9E-05	1.0E+03	1.5E-05	2.1E-05	3.4E-03	0.72	6.75	1.3E+10	9.6E+09	249.62	0.95	0.29	0.29
54	48	21.8	21.5	21.28	2.6E-02	1.2E+00	1.9E-05	1.0E+03	1.5E-05	2.1E-05	3.4E-03	0.72	6.75	1.1E+10	8.1E+09	236.14	0.90	0.23	0.23
57	3	20.7	20.3	19.93	2.6E-02	1.2E+00	1.8E-05	1.0E+03	1.5E-05	2.1E-05	3.4E-03	0.72	6.75	1.7E+10	1.2E+10	268.60	1.02	0.39	0.39
57	6	23.0	21.5	19.93	2.6E-02	1.2E+00	1.8E-05	1.0E+03	1.5E-05	2.1E-05	3.4E-03	0.72	6.75	6.7E+10	4.8E+10	417.13	1.59	2.44	2.44
57	9	24.9	22.4	19.93	2.6E-02	1.2E+00	1.8E-05	1.0E+03	1.5E-05	2.1E-05	3.4E-03	0.72	6.75	1.1E+11	7.8E+10	486.75	1.85	4.61	4.61
57	12	23.7	21.8	19.93	2.6E-02	1.2E+00	1.8E-05	1.0E+03	1.5E-05	2.1E-05	3.4E-03	0.72	6.75	8.3E+10	5.9E+10	445.48	1.70	3.20	3.20
57	15	26.2	23.2	20.27	2.6E-02	1.2E+00	1.8E-05	1.0E+03	1.5E-05	2.1E-05	3.4E-03	0.72	6.75	1.3E+11	9.3E+10	514.52	1.96	5.81	5.81
57	18	29.9	25.1	20.27	2.6E-02	1.2E+00	1.8E-05	1.0E+03	1.5E-05	2.1E-05	3.4E-03	0.72	6.75	2.1E+11	1.5E+11	601.36	2.29	11.02	11.02
57	21	28.5	24.4	20.27	2.6E-02	1.2E+00	1.8E-05	1.0E+03	1.5E-05	2.1E-05	3.4E-03	0.72	6.75	1.8E+11	1.3E+11	571.70	2.18	8.96	8.96
57	24	30.0	25.1	20.27	2.6E-02	1.2E+00	1.8E-05	1.0E+03	1.5E-05	2.1E-05	3.4E-03	0.72	6.75	2.1E+11	1.5E+11	603.36	2.30	11.18	11.18
57	27	33.1	26.7	20.27	2.6E-02	1.2E+00	1.8E-05	1.0E+03	1.5E-05	2.1E-05	3.4E-03	0.72	6.75	2.8E+11	2.0E+11	659.63	2.51	16.11	16.11
57	30	23.8	22.0	20.27	2.6E-02	1.2E+00	1.8E-05	1.0E+03	1.5E-05	2.1E-05	3.4E-03	0.72	6.75	7.7E+10	5.5E+10	435.67	1.66	2.93	2.93
57	33	23.8	22.0	20.27	2.6E-02	1.2E+00	1.8E-05	1.0E+03	1.5E-05	2.1E-05	3.4E-03	0.72	6.75	7.7E+10	5.5E+10	435.67	1.66	2.93	2.93
57	36	23.7	22.0	20.27	2.6E-02	1.2E+00	1.8E-05	1.0E+03	1.5E-05	2.1E-05	3.4E-03	0.72	6.75	7.5E+10	5.4E+10	431.68	1.64	2.82	2.82
57	39	21.4	21.3	21.28	2.6E-02	1.2E+00	1.9E-05	1.0E+03	1.5E-05	2.1E-05	3.4E-03	0.72	6.75	2.6E+09	1.9E+09	149.18	0.57	0.03	0.03
60	0	20.1	20.0	19.93	2.6E-02	1.2E+00	1.8E-05	1.0E+03	1.5E-05	2.1E-05	3.4E-03	0.72	6.75	3.7E+09	2.7E+09	167.05	0.64	0.05	0.05
60	3	20.5	20.2	19.93	2.6E-02	1.2E+00	1.8E-05	1.0E+03	1.5E-05	2.1E-05	3.4E-03	0.72	6.75	1.2E+10	9.0E+09	244.24	0.93	0.27	0.27
60	6	21.7	20.8	19.93	2.6E-02	1.2E+00	1.8E-05	1.0E+03	1.5E-05	2.1E-05	3.4E-03	0.72	6.75	3.9E+10	2.8E+10	349.88	1.33	1.18	1.18
60	9	24.3	22.1	19.93	2.6E-02	1.2E+00	1.8E-05	1.0E+03	1.5E-05	2.1E-05	3.4E-03	0.72	6.75	9.6E+10	6.9E+10	467.07	1.78	3.89	3.89
60	12	27.2	23.6	19.93	2.6E-02	1.2E+00	1.8E-05	1.0E+03	1.5E-05	2.1E-05	3.4E-03	0.72	6.75	1.6E+11	1.1E+11	550.00	2.09	7.61	7.61
60	15	27.5	23.9	20.27	2.6E-02	1.2E+00	1.8E-05	1.0E+03	1.5E-05	2.1E-05	3.4E-03	0.72	6.75	1.6E+11	1.1E+11	548.36	2.09	7.55	7.55
60	18	22.9	21.6	20.27	2.6E-02	1.2E+00	1.8E-05	1.0E+03	1.5E-05	2.1E-05	3.4E-03	0.72	6.75	5.7E+10	4.1E+10	396.53	1.51	1.99	1.99
60	21	24.9	22.6	20.27	2.6E-02	1.2E+00	1.8E-05	1.0E+03	1.5E-05	2.1E-05	3.4E-03	0.72	6.75	1.0E+11	7.3E+10	475.23	1.81	4.19	4.19
60	24	29.9	25.1	20.27	2.6E-02	1.2E+00	1.8E-05	1.0E+03	1.5E-05	2.1E-05	3.4E-03	0.72	6.75	2.1E+11	1.5E+11	601.36	2.29	11.02	11.02
60	27	32.1	26.2	20.27	2.6E-02	1.2E+00	1.8E-05	1.0E+03	1.5E-05	2.1E-05	3.4E-03	0.72	6.75	2.6E+11	1.9E+11	642.59	2.45	14.47	14.47
63	6	21.2	20.6	19.93	2.6E-02	1.2E+00	1.8E-05	1.0E+03	1.5E-05	2.1E-05	3.4E-03	0.72	6.75	2.8E+10	2.0E+10	314.80	1.20	0.76	0.76
63	9	23.8	21.9	19.93	2.6E-02	1.2E+00	1.8E-05	1.0E+03	1.5E-05	2.1E-05	3.4E-03	0.72	6.75	8.5E+10	6.1E+10	449.23	1.71	3.31	3.31
63	12	24.8	22.4	19.93	2.6E-02	1.2E+00	1.8E-05	1.0E+03	1.5E-05	2.1E-05	3.4E-03	0.72	6.75	1.1E+11	7.7E+10	483.58	1.84	4.48	4.48
63	15	28.8	24.5	20.27	2.6E-02	1.2E+00	1.8E-05	1.0E+03	1.5E-05	2.1E-05	3.4E-03	0.72	6.75	1.9E+11	1.3E+11	578.32	2.20	9.39	9.39
63	18	22.0	21.1	20.27	2.6E-02	1.2E+00	1.8E-05	1.0E+03	1.5E-05	2.1E-05	3.4E-03	0.72	6.75	3.8E+10	2.7E+10	346.92	1.32	1.14	1.14
63	21	23.0	21.6	20.27	2.6E-02	1.2E+00	1.8E-05	1.0E+03	1.5E-05	2.1E-05	3.4E-03	0.72	6.75	6.0E+10	4.3E+10	401.28	1.53	2.09	2.09

x	y	T_{20}	T_f	T_∞	k	ρ	μ	C_p	ν	α	β	Pr	L	Gr	Ra	Nu_L	h	q_{adv}	q_{cond}
63	24	22.3	21.3	20.27	2.6E-02	1.2E+00	1.8E-05	1.0E+03	1.5E-05	2.1E-05	3.4E-03	0.72	6.75	4.4E+10	3.2E+10	365.06	1.39	1.41	1.41
63	27	21.4	20.8	20.27	2.6E-02	1.2E+00	1.8E-05	1.0E+03	1.5E-05	2.1E-05	3.4E-03	0.72	6.75	2.5E+10	1.8E+10	302.97	1.15	0.65	0.65
66	3	20.0	20.0	19.93	2.6E-02	1.2E+00	1.8E-05	1.0E+03	1.5E-05	2.1E-05	3.4E-03	0.72	6.75	1.5E+09	1.1E+09	126.82	0.48	0.02	0.02
66	6	23.9	21.9	19.93	2.6E-02	1.2E+00	1.8E-05	1.0E+03	1.5E-05	2.1E-05	3.4E-03	0.72	6.75	8.7E+10	6.3E+10	452.92	1.72	3.42	3.42
66	9	23.8	21.9	19.93	2.6E-02	1.2E+00	1.8E-05	1.0E+03	1.5E-05	2.1E-05	3.4E-03	0.72	6.75	8.5E+10	6.1E+10	449.23	1.71	3.31	3.31
66	12	26.0	23.0	19.93	2.6E-02	1.2E+00	1.8E-05	1.0E+03	1.5E-05	2.1E-05	3.4E-03	0.72	6.75	1.3E+11	9.6E+10	519.02	1.98	6.00	6.00
66	15	21.1	20.7	20.27	2.6E-02	1.2E+00	1.8E-05	1.0E+03	1.5E-05	2.1E-05	3.4E-03	0.72	6.75	1.8E+10	1.3E+10	274.73	1.05	0.43	0.43
66	18	20.4	20.3	20.27	2.6E-02	1.2E+00	1.8E-05	1.0E+03	1.5E-05	2.1E-05	3.4E-03	0.72	6.75	2.8E+09	2.0E+09	153.48	0.58	0.04	0.04
66	57	25.0	23.3	21.62	2.6E-02	1.2E+00	1.9E-05	1.0E+03	1.5E-05	2.1E-05	3.4E-03	0.72	6.75	7.2E+10	5.2E+10	427.59	1.63	2.75	2.75
66	69	23.0	22.3	21.62	2.6E-02	1.2E+00	1.9E-05	1.0E+03	1.5E-05	2.1E-05	3.4E-03	0.72	6.75	3.0E+10	2.1E+10	321.30	1.22	0.84	0.84
69	3	20.0	20.0	19.93	2.6E-02	1.2E+00	1.8E-05	1.0E+03	1.5E-05	2.1E-05	3.4E-03	0.72	6.75	1.5E+09	1.1E+09	126.82	0.48	0.02	0.02
69	6	20.1	20.0	19.93	2.6E-02	1.2E+00	1.8E-05	1.0E+03	1.5E-05	2.1E-05	3.4E-03	0.72	6.75	3.7E+09	2.7E+09	167.05	0.64	0.05	0.05
69	9	23.0	21.5	19.93	2.6E-02	1.2E+00	1.8E-05	1.0E+03	1.5E-05	2.1E-05	3.4E-03	0.72	6.75	6.7E+10	4.8E+10	417.13	1.59	2.44	2.44
69	12	23.6	21.8	19.93	2.6E-02	1.2E+00	1.8E-05	1.0E+03	1.5E-05	2.1E-05	3.4E-03	0.72	6.75	8.0E+10	5.8E+10	441.66	1.68	3.09	3.09
69	15	20.5	20.4	20.27	2.6E-02	1.2E+00	1.8E-05	1.0E+03	1.5E-05	2.1E-05	3.4E-03	0.72	6.75	5.0E+09	3.6E+09	183.39	0.70	0.08	0.08
69	60	21.9	21.8	21.62	2.6E-02	1.2E+00	1.9E-05	1.0E+03	1.5E-05	2.1E-05	3.4E-03	0.72	6.75	6.0E+09	4.3E+09	194.13	0.74	0.10	0.10
69	63	21.7	21.7	21.62	2.6E-02	1.2E+00	1.9E-05	1.0E+03	1.5E-05	2.1E-05	3.4E-03	0.72	6.75	1.7E+09	1.2E+09	131.40	0.50	0.02	0.02
69	66	22.4	22.0	21.62	2.6E-02	1.2E+00	1.9E-05	1.0E+03	1.5E-05	2.1E-05	3.4E-03	0.72	6.75	1.7E+10	1.2E+10	268.10	1.02	0.40	0.40
69	69	22.0	21.8	21.62	2.6E-02	1.2E+00	1.9E-05	1.0E+03	1.5E-05	2.1E-05	3.4E-03	0.72	6.75	8.1E+09	5.9E+09	213.67	0.81	0.15	0.15
72	3	20.8	20.4	19.93	2.6E-02	1.2E+00	1.8E-05	1.0E+03	1.5E-05	2.1E-05	3.4E-03	0.72	6.75	1.9E+10	1.4E+10	279.19	1.06	0.46	0.46
72	66	22.2	21.9	21.62	2.6E-02	1.2E+00	1.9E-05	1.0E+03	1.5E-05	2.1E-05	3.4E-03	0.72	6.75	1.2E+10	8.9E+09	244.13	0.93	0.27	0.27
72	69	21.7	21.7	21.62	2.6E-02	1.2E+00	1.9E-05	1.0E+03	1.5E-05	2.1E-05	3.4E-03	0.72	6.75	1.7E+09	1.2E+09	131.40	0.50	0.02	0.02
72	72	22.0	21.8	21.62	2.6E-02	1.2E+00	1.9E-05	1.0E+03	1.5E-05	2.1E-05	3.4E-03	0.72	6.75	8.1E+09	5.9E+09	213.67	0.81	0.15	0.15

Appendix C

Bravo shallow ground temperatures

TABLE C.1: Bravo shallow ground temperatures

x	y	T (°C)	x	y	T (°C)	x	y	T (°C)	x	y	T (°C)
0	0	20.2	9	6	17.8	18	12	15.3	27	18	16.8
0	3	22.3	9	9	17.3	18	15	15.8	27	21	19.6
0	6	23.7	9	12	16.9	18	18	17.2	27	24	20.8
0	27	20.9	9	33	22.6	18	39	26	27	45	32.9
0	30	18.8	9	36	21.6	18	42	24.9	27	48	24
0	33	18.1	9	39	20.2	18	45	23.3	27	51	20.1
0	54	16.2	9	60	17.8	18	66	17.7	27	72	18.1
0	57	15.7	9	63	16.9	18	69	16.7	66	72	21
0	60	16.9	9	66	17.7	18	72	17.4	69	69	22
3	0	18.9	12	6	17.6	21	12	15.6	30	18	17.6
3	3	17.7	12	9	18	21	15	16.1	30	21	19.4
3	6	18.3	12	12	17.4	21	18	18	30	24	NA
3	27	21	12	33	22.9	21	39	NA	30	45	27.1
3	30	19.7	12	36	22.4	21	42	27.1	30	48	23.9
3	33	18.3	12	39	22.2	21	45	22.3	30	51	17.8
3	54	16.4	12	60	16.5	21	66	17.1	30	72	16.8
3	57	16	12	63	17.8	21	69	16.9	69	72	20.9
3	60	17.8	12	66	18.1	21	72	16.9	72	69	21.7
6	0	19.9	15	6	16.4	24	12	15.5	33	18	16.8
6	3	19.3	15	9	16.9	24	15	17.1	33	21	18.9
6	6	21.3	15	12	16.6	24	18	20.3	33	24	20.5
6	27	20.8	15	33	24.9	24	39	NA	33	45	19.5
6	30	19.8	15	36	23.2	24	42	28.2	33	48	19.3
6	33	20.4	15	39	23.9	24	45	26.3	33	51	17.1
6	54	16.6	15	60	16	24	66	17.4	33	72	15.9
6	57	15.9	15	63	16.7	24	69	16.5	72	72	22
9	0	18.2	18	6	15.9	27	12	17	36	18	16.4
9	3	18.2	18	9	15.6	27	15	17.3	36	21	16.8
9	27	21	18	33	24.2	27	39	NA	36	45	17.8
9	30	21.6	18	36	24	27	42	NA	36	48	16.7
9	54	15.6	18	60	16	27	66	16.6	36	72	15.3
9	57	15.4	18	63	16.9	27	69	16.6	39	69	15.3
12	0	18.2	21	6	15.8	30	12	15.4	0	21	22.1
12	3	17.8	21	9	15.2	30	15	16.9	0	24	21.8
12	27	21.7	21	33	26.7	30	39	NA	0	48	18.4
12	30	22.3	21	36	NA	30	42	28.3	0	51	17.1
12	54	16.6	21	60	15.8	30	66	16.2	39	72	15.5
12	57	15.8	21	63	16.5	30	69	15.8	42	69	15.5
15	0	16.3	24	6	15.8	33	12	14.9	3	21	21.8
15	3	22.2	24	9	16.3	33	15	16.5	3	24	22.6
15	27	23.4	24	33	NA	33	39	29.3	3	48	16.2
15	30	24.6	24	36	NA	33	42	22	3	51	16.3
15	54	17.6	24	60	16.1	33	66	15.4	42	72	15.6
15	57	15.8	24	63	17	33	69	15	45	69	14.9
18	0	16.2	27	6	16.2	36	12	15	6	21	21.6
18	3	15.6	27	9	16.1	36	15	15.5	6	24	22.2
18	27	23	27	33	NA	36	39	23.1	6	48	16.2
18	30	23.8	27	36	NA	36	42	24.9	6	51	16.1

TABLE C.1: Bravo shallow ground temperatures

x	y	T (°C)	x	y	T (°C)	x	y	T (°C)	x	y	T (°C)
18	54	16.6	27	60	15.8	36	66	15.9	45	72	15.2
18	57	16.1	27	63	15.9	36	69	15	48	69	16.4
21	0	16.2	30	6	15.9	0	15	20.4	9	21	20
21	3	16.6	30	9	15.2	0	18	22	9	24	20.6
21	27	22.9	30	33	NA	0	42	16.5	9	48	15.9
21	30	22.5	30	36	NA	0	45	17.1	9	51	15.8
21	54	16.5	30	60	15.5	0	69	16.5	48	72	16.3
21	57	15.7	30	63	16	0	72	17.9	51	69	15.7
24	0	18.8	33	6	16.4	3	15	18.7	12	21	18.6
24	3	16.5	33	9	15.5	3	18	20	12	24	20.7
24	27	22.5	33	33	29.8	3	42	16	12	48	17.4
24	30	22.8	33	36	NA	3	45	16	12	51	16.9
24	54	16.9	33	60	15.3	3	69	16.9	51	72	15.8
24	57	15.6	33	63	15.4	3	72	17.3	54	69	17.6
27	0	19.3	36	6	16.7	6	15	21.4	15	21	19.1
27	3	16.8	36	9	15.9	6	18	21.6	15	24	20.6
27	27	22.3	36	33	25.6	6	42	17.4	15	48	17.3
27	30	22.8	36	36	NA	6	45	17.6	15	51	16.9
27	54	16.7	36	60	16	6	69	17.9	54	72	16
27	57	16.2	36	63	15.6	6	72	18.4	57	69	17.6
30	0	18.7	0	9	23.1	9	15	17.8	18	21	24.4
30	3	16	0	12	18.7	9	18	17.8	18	24	20.8
30	27	26.1	0	36	17.9	9	42	18.1	18	48	20.6
30	30	23.3	0	39	17	9	45	17.6	18	51	17.8
30	54	16.8	0	63	15.4	9	69	18	57	72	16.3
30	57	16	0	66	17	9	72	18.9	60	69	19.9
33	0	18.4	3	9	20.1	12	15	17	21	21	20.6
33	3	17.2	3	12	18.5	12	18	16.3	21	24	21.2
33	27	20.3	3	36	17.3	12	42	20.8	21	48	24.4
33	30	20.6	3	39	17.5	12	45	19.7	21	51	19.4
33	54	16.4	3	63	17.2	12	69	18.8	60	72	18.2
33	57	15.4	3	66	16.7	12	72	19.3	63	69	20.8
36	0	18.2	6	9	18.2	15	15	15.4	24	21	22.5
36	3	17.9	6	12	18.3	15	18	17.7	24	24	19.9
36	27	22	6	36	21.4	15	42	25	24	48	23.3
36	30	23.8	6	39	18.3	15	45	22.5	24	51	19.4
36	51	16.5	6	60	16.9	15	66	17	24	72	17
36	54	15.9	6	63	18.1	15	69	17.5	63	72	19.7
36	57	15.8	6	66	17.1	15	72	18.7	66	69	23
39	6	18.8	54	0	22	48	3	23	57	3	20.7
39	66	15.4	54	60	19	69	54	20	48	45	18.9
39	63	16.7	54	57	17.8	69	51	20	48	42	18.3
39	60	16.4	54	54	16.3	69	48	20.3	48	39	20.2
39	36	20	54	30	24.9	69	24	19.7	48	15	20.7
39	33	19.3	54	27	29.5	69	21	18.7	48	12	25.6
39	30	19.6	54	24	33.5	69	18	18.9	48	9	28.5
42	6	19.2	57	0	18.8	51	3	24.1	60	3	20.5
42	66	15.2	57	60	17.9	72	54	21.5	51	45	20.7
42	63	15.9	57	57	18.8	72	51	20.3	51	42	18.3
42	60	17.8	57	54	17.6	72	48	19.6	51	39	19.8
42	36	19.3	57	30	23.8	72	24	20	51	15	23.2
42	33	19.7	57	27	33.1	72	21	18.7	51	12	25.5

TABLE C.1: Bravo shallow ground temperatures

x	y	T (°C)	x	y	T (°C)	x	y	T (°C)	x	y	T (°C)
45	66	15.1	60	60	19.3	39	51	16.3	54	45	21.9
45	63	15.9	60	57	20.9	39	48	17.9	54	42	19.4
45	60	17.6	60	54	19.4	39	45	17.6	54	39	25.2
45	36	18	60	30	19.2	39	21	17.5	54	15	27.6
45	33	19.1	60	27	32.1	39	18	16.3	54	12	27.9
45	6	21.6	60	0	20.1	54	3	25.7	63	3	19.9
48	66	16.3	63	60	20.3	42	51	16.9	57	45	19.2
48	63	17.9	63	57	21.6	42	48	16.2	57	42	20.4
48	60	17.6	63	54	20.8	42	45	17	57	39	21.4
48	36	20.6	63	30	19.4	42	21	18.3	57	15	26.2
48	33	22.9	63	27	21.4	42	18	16.9	57	12	23.7
51	66	16.9	66	60	21.5	45	51	16.5	60	45	20.3
51	63	17.2	66	57	25	45	48	16.2	60	42	19.5
51	60	17.3	66	54	18.9	45	45	16.9	60	39	20.4
51	36	24.3	66	30	20.1	45	21	20.7	60	15	27.5
51	33	21.6	66	27	19.7	45	18	21.3	60	12	27.2
51	9	26.2	66	3	20	60	6	21.7	63	0	19.9
54	66	18	69	60	21.9	48	51	19	63	45	19.8
54	63	18.5	69	57	21.4	48	48	17.5	63	42	19.5
54	36	24	69	30	18.8	48	21	28.1	63	15	28.8
54	33	23.4	69	27	19.8	48	18	20.4	63	12	24.8
54	9	27.3	69	3	20	63	6	21.2	66	0	19.4
57	66	17.6	72	60	21.5	51	51	16.5	66	45	19.8
57	63	18	72	57	20.9	51	48	18.4	66	42	18.9
57	36	23.7	72	30	17.9	51	21	29.6	66	15	21.1
57	33	23.8	72	27	18.8	51	18	26.3	66	12	26
57	9	24.9	72	3	20.8	66	6	23.9	69	0	19.9
60	66	19.2	39	57	16.2	54	51	17.9	69	45	19.7
60	63	19.7	39	54	17.6	54	48	21.8	69	42	19.2
60	36	20	39	27	20.2	54	21	30.1	69	15	20.5
60	33	18.9	39	24	18.3	54	18	27.2	69	12	23.6
60	9	24.3	39	0	19.7	69	6	20.1	72	0	19.6
63	66	20.5	42	57	17.2	57	51	17.6	72	45	19.2
63	63	19.9	42	54	17.3	57	48	19.9	72	42	19.5
63	39	18.8	42	30	19.4	57	24	30	72	18	18.1
63	36	19.4	42	27	19.7	57	21	28.5	72	15	18.9
63	33	20.2	42	24	18.1	57	18	29.9	72	12	18.4
63	9	23.8	42	0	21.9	72	6	19.2	48	6	26.5
66	9	23.8	45	0	21.5	39	3	18.6	51	6	23.3
66	66	21.6	45	57	20.2	60	51	18	39	42	18.5
66	63	21	45	54	16.9	60	48	19.9	39	39	19
66	39	19	45	30	20.3	60	24	29.9	39	15	15.8
66	36	20	45	27	19.2	60	21	24.9	39	12	17.9
66	33	19.9	45	24	20.8	60	18	22.9	39	9	17.9
69	9	23	48	0	23.1	42	3	19.9	54	6	26.3
69	66	22.4	48	57	16.8	63	51	18.2	42	42	16.5
69	63	21.7	48	54	17.9	63	48	19.5	42	39	18.9
69	39	18.4	48	30	21.2	63	24	22.3	42	15	18
69	36	19	48	27	21.5	63	21	23	42	12	18.1
69	33	18.1	48	24	25.5	63	18	22	42	9	18.8
72	9	18.6	51	0	26.6	45	3	22	57	6	23
72	66	22.2	51	57	17	66	51	19.9	45	42	16.1

TABLE C.1: Bravo shallow ground temperatures

x	y	T (°C)	x	y	T (°C)	x	y	T (°C)	x	y	T (°C)
72	63	21	51	54	16.5	66	48	19.8	45	39	18
72	39	18.3	51	30	21.5	66	24	19.7	45	15	17
72	36	19.2	51	27	23.6	66	21	20.1	45	12	19.1
72	33	16.7	51	24	27.2	66	18	20.4	45	9	22.3

Appendix D

Publication Permission for Chapter 1

Transactions article

Brian Schmidt <bschmidt@geothermal.org>   Mon, Apr 30, 2018 at 8:24 AM
To: Cary Lindsey <caryrlindsey@gmail.com>

Hello Cary,

Thank you for checking in with us regarding your publication.

GRC only claims copyright on the collective work *Transactions*; our authors retain the rights to their individual contributions. The only time you would need additional permissions from us would be if you were using our actual published version or some aspect of it – e.g. the figures and/or formatting. And we generally grant authors any such permission when. To be safe, however, you should also obtain the permission of your co-authors, as they have also retained the rights to their contributions.

The Geothermal Resources Council grants you permission to use, in entirety or part, any aspects that we retain rights to, of the paper "Ice Box Calorimetry: A Test of Applicability in Non-Steaming Geothermal Areas" in the publication of your thesis. Our only request is that it's original publication source be cited somewhere in the document.

Please let me know if you need something more formal than this, I can draw up an actual letter if need be.

Best regards,

Brian

Brian Schmidt
Librarian and Geothermal Industry Analyst
Geothermal Resources Council
Davis, California 95617